A GEOLOGIC CHARACTERIZATION OF THE ALONGSHORE VARIABILITY IN BEACH-DUNE MORPHOLOGY: PADRE ISLAND NATIONAL SEASHORE, TEXAS

A Thesis

by

BRADLEY ALLEN WEYMER

Submitted to the Office of Graduate Studies of
Texas A&M University
in partial fulfillment of the requirements for the degree of

MASTER OF SCIENCE

May 2012

Major Subject: Geology

A Geologic Characterization of the Alongshore Variability in Beach-Dune Morphology: Padre Island National Seashore, Texas

A GEOLOGIC CHARACTERIZATION OF THE ALONGSHORE VARIABILITY IN BEACH-DUNE MORPHOLOGY: PADRE ISLAND NATIONAL SEASHORE, TEXAS

A Thesis

by

BRADLEY ALLEN WEYMER

Submitted to the Office of Graduate Studies of
Texas A&M University
in partial fulfillment of the requirements for the degree of

MASTER OF SCIENCE

Approved by:

Co-Chairs of Committee, John R. Giardino
Chris Houser
Committee Member, Timothy Dellapenna
Head of Department, John R. Giardino

May 2012

Major Subject: Geology

ABSTRACT

A Geologic Characterization of the Alongshore Variability in Beach-Dune Morphology:

Padre Island National Seashore, Texas. (May 2012)

Bradley Allen Weymer, B.S., Millersville University

Co-Chairs of Advisory Committee: Dr. John R. Giardino
Dr. Chris Houser

The alongshore variability of beach-dune systems and the response and recovery from extreme storms remains poorly understood. The height and extent of foredunes along barrier islands varies over a range of spatial scales, implying that during extreme storms, the beach-dune system should respond in different ways depending on the elevation and volume of the dunes relative to the storm surge. The purpose of this study is to use Ground-Penetrating Radar (GPR) and vibra-cores to investigate the internal structure of small, intermediate and large dunes along a 2.5 km transect of beach in Padre Island National Seashore, TX with particular attention to storm impacts. A series of dune normal and parallel GPR profiles were collected to capture the variation in beach-dune morphology at the three sites. Site locations were chosen along a transition from dissipative to intermediate beach states. Following the Sallenger (2000) storm impact model, the small dune is defined by low-lying topography that is susceptible to overwash and inundation depending on the size of the storm surge. The large dune is characteristic of the “collision regime”, while the intermediate dune represents a transition between “overwash” and “collision regimes”, with the underlying assumption

that all three dunes would be impacted by the same level of surge during a single storm event. Results from the GPR survey suggest that each site contains a bright, laterally continuous radar reflector that is interpreted with the aid of the sedimentary data as an erosional layer. Different characteristic radar facies and sequence boundaries provide evidence as to how each dune evolved through and after the storm. Results from XRF scans and grain size analysis show a direct comparison between the GPR reflectors at the storm surface and spikes in calcium counts from XRF scans to distinct changes in grain size parameters at the same depth. It is argued that the location of each shell layer corresponds to a storm surface generated during a single storm, which means it is possible to interpret different recovery mechanisms. The presence of the storm layer across the backbeach and dunes provides evidence for the height and extent of the surge during the storm event. The data suggests that the small dune was overtopped by the surge, experiencing minimal erosion and recovery. The intermediate dune was completely eroded by the surge, but showed the greatest recovery of all the dune sites. The large dune was scoured at the base with marginal impact along its crest and shows minimal recovery after the storm. These results suggest that the evolution (i.e., transgression) of a barrier island varies considerably over short distances.

DEDICATION

To my family and friends, thank you for always being there.
I dedicate this manuscript to my grandfathers;
Horace J. Weymer and James T. Morton.

ACKNOWLEDGEMENTS

I would like to thank my co-chairs, Dr. Rick Giardino and Dr. Chris Houser, and committee member, Dr. Tim Dellapenna, for their guidance and support throughout the course of this research. I especially express my sincere gratitude for my supervisors Dr. Brad Clement, Dr. John V. Firth, Phil Rumford and Bill Wasson at the Integrated Ocean Drilling Program (IODP) for providing funding support through the San Andreas Fault Observatory at Depth (SAFOD) research grant. I will forever be indebted to their unwavering generosity and for giving me the opportunity to pursue my dream of becoming a graduate student. I especially thank Dr. Debbie Thomas for her guidance and support since beginning my academic journey at Texas A&M. I thank Dr. Robert Weiss for his support during my first year in graduate school. A very special thanks to Dr. Mark Everett and Dr. Doug Sasson for their expertise in GPR data acquisition and processing. I thank Dr. Doug Sherman for numerous encouraging conversations regarding my research. I would like to thank Brian and Daniel Labude, Gemma Barrett and Renee Francese for their hard work and dedication in the field and many stimulating conversations. I thank Eugene Farrell for his guidance and expertise with the grain size analysis. I thank David Houpt, Thomas Gorgas and YuliaVasilyeva at (IODP) and Dr. Mitch Lyle for their recommendations and expertise in XRF scanning and data interpretation. Additionally, I would like to thank Antonio Pereira for processing the XRD samples. And lastly, to my parents Rick and Beth Weymer, sisters Hilary Thompson and Bethany Weymer and my fiancé Ruifang Xie for their unconditional

love, understanding and patience. This study was supported in part by the National Science Foundation under award number GSS-0920851 (to Dr. Chris Houser) and by the National Park Service permit number PAIS-2010-SCI-0020.

TABLE OF CONTENTS

Page

LIST OF FIGURES

FIGURE Page

FIGURE Page

LIST OF TABLES

INTRODUCTION AND PROBLEM STATEMENT

The impact of extreme storms along sandy beaches depends on the height and extent of the foredunes relative to the elevation of the storm surge (Sallenger, 2000). The impacts change with increasing storm surge from beach erosion to dune erosion, thus, governing how sediment is transferred across the beach-dune system. The evolution of beach-dune systems remains poorly understood. To address this problem,a geologic study that used ground-penetrating radar (GPR) and vibra-cores was undertaken to characterize beach-dune morphology between small, intermediate and large dunes along the northern segment of Padre Island National Seashore, Texas.

Numerous GPR studies have investigated beach-dune interaction along a single, two-dimensional cross-shore transect or across beaches in different locations altogether (Bailey and Bristow, 2000; Bristow and Bailey, 2001; Bristow et al., 2000b; Buynevich et al., 2007a; McGourty and Wilson, 2000). However, there is a paucity of data to describe how beach-dune evolution varies over short distances along the same beach. Typically, dissipative beaches are backed by large dunes, whereas reflective beaches normally favor small dunes as wave energy is reflected back from a narrower, steep-angle, coarse-grained beach and swash-zone (Short and Hesp, 1982). Because of fundamental differences between the morphodynamic beach states, the beach-dune systems between dissipative, intermediate and reflective beaches should be different. Nevertheless, along the same beach it is possible to find transitions between beach states

---

This thesis follows the style of Geomorphology.

that may influence dune development and response of the beach-dune system to extreme storms.

This project completed a geologic characterization of the beach-dune interface for small, intermediate and large dunes, which may have been impacted by the same storm in different ways. Variations between the interpreted internal structures of the dunes can be used to characterize the degree of impact from storms. In other words, by identifying erosional surfaces (i.e., storm surfaces) within the dunes in the context of inundation, overwash and collision regimes, this project describes how the beach and dune systems interact and what is important regarding these interactions to island transgression. The purpose of this project is to conduct a geologic study that uses ground-penetrating radar (GPR) and vibra-cores to:

1. Characterize alongshore variation in beach-dune morphology for different-sized dunes.
2. Interpret internal structures within the beach-dune system with attention to a transgressing barrier islands response and recovery from storms.

To achieve the objectives of the study, dune-normal and dune-parallel GPR transects were surveyed to create a three-dimensional internal view of large, intermediate and small dunes assuming this can be used to determine whether there are different transgression histories of the beach-dune system within a 2.5 km stretch of Padre Island National Seashore. Additionally, twelve vibra-cores collected along the main GPR transects (four at each site) provided internal views for the upper meter of the GPR profiles that could not be interpreted because of interference between the 200 MHz antennae. From the vibra-cores, core descriptions, grain size analysis and (X-Ray

Fluorescence) XRF data were collected to categorize textural properties of the sediment and identify storm layers within the cores. Thus, the vibra-cores provided supporting evidence of the interpreted storm surface identified in the GPR profiles. The results from GPR surveys, grain size analysis and XRF data confirm that a distinct storm surface persists at a depth of 120 cm along the backbeach at each study site. The difference in dune height between each site means that the beach-dune system was impacted by the same storm in different ways within a relatively small area.

PADRE ISLAND NATIONAL SEASHORE STUDY AREA

Padre Island, a Holocene barrier island, is thought to have formed 5,000 BP(Fisk, 1959). The island extends from the southern edge of Mustang Island in the north to the Mansfield Channel, which separates North Padre Island from South Padre Island (Figure 1). It is the longest barrier island in the United States at 182 km in length. Padre Island is separated from the mainland by Laguna Madre, a hypersaline lagoon. North Padre Island is micro-tidal with a mean diurnal tidal range of approximately 0.43 m (Weise, 1980). The northern segment of Padre Island is comprised of a double-barred beach profile, resulting in a predominately dissipative beach state as a function of wide, low-angle beach and surf-zone geometry. The beach is comprised of fine-grained sands and influenced by prevailing southeasterly winds, with a mean speed of 10-12 knots. The study site is located within the protected portion of the beach between the South Beach access road (Park Road 22) extending 2.5 km north in close proximity to the Malaquite Beach campsite (Figure 1). This portion of the beach is part of the restricted area where the National Park Service does not allow public vehicles to drive along the beach between the entrance to South Beach (Park Rd. 22) and the North Beach access road. Three sites within a 2.5 km stretch of the study area were chosen for the GPR survey. Site 1 represents an intermediate-sized dune that is defined as having a height between 2-3.5 m. The smallest dune (less than 2 m) is located at Site 2 and the largest dune at Site 3 (greater than 3.5 m) represents the other end member.

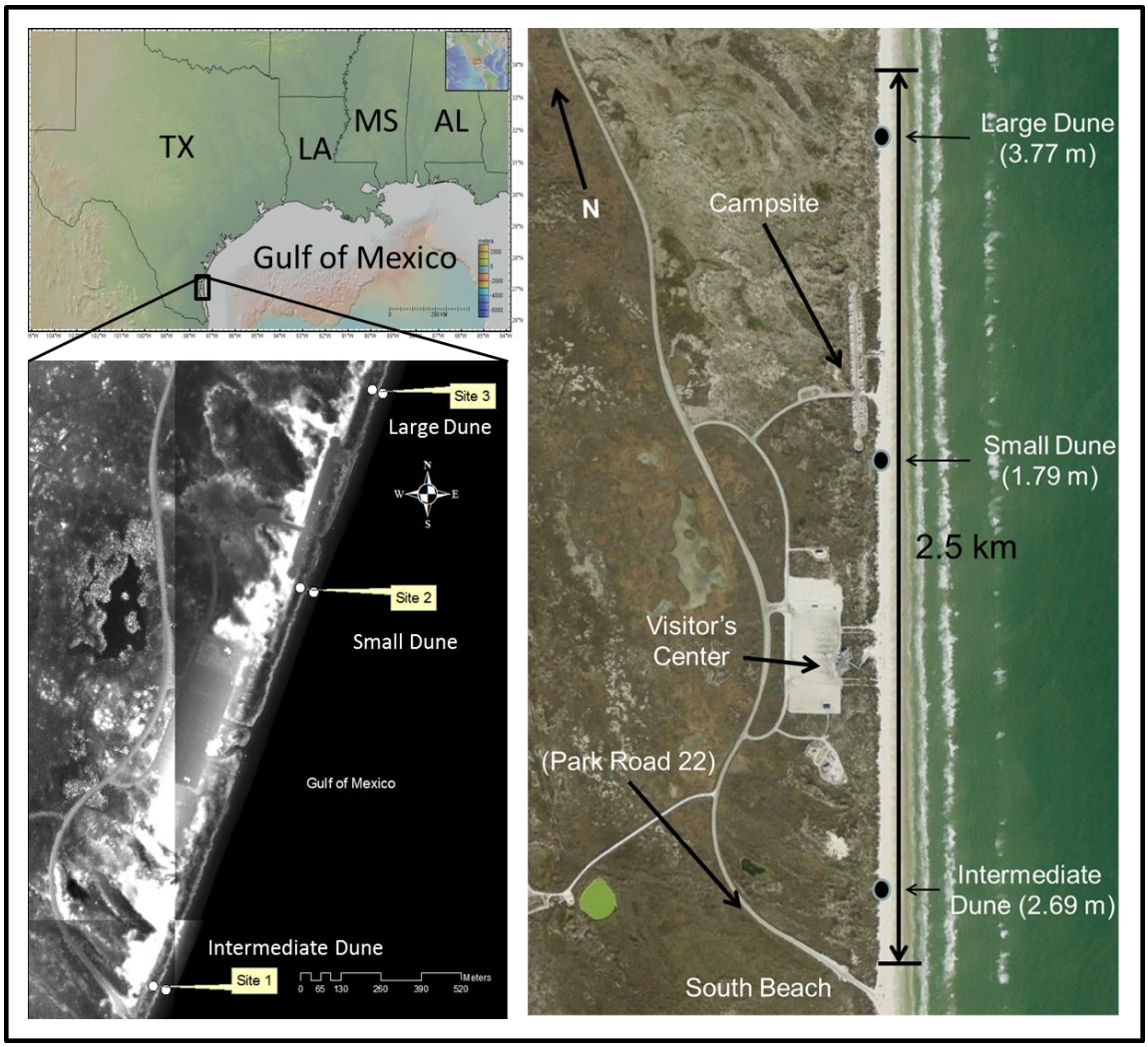

Figure 1. Location map showing aerial LiDAR image from December, 2010 (Courtesy National Park Service) and satellite image of the three study sites (Modified from Google Earth™ 2011, GeoMapApp© 2011).

The climate along the coastal region of southern Texas ranges from semi-arid to temperate with an average annual temperature of 22.2° C (72° F) and an average annual rainfall of 74 cm (29.13 in). Hurricanes and tropical cyclones impact the Texas coast at an average rate of 0.67 storms per year, or two storms every three years (Weise, 1980).

During the last fifty years, Padre Island was struck by Hurricane Beulah (1967), Hurricane Allen (1980), Hurricane Bret (1999) and Hurricane Dolly (2008).

The primary sediment source for north Padre Island originates from the Mississippi River. Longshore currents along the island are from south to north. Distribution of heavy minerals and bimodal grain size modes identified by Hayes (1964) suggest that along the middle section of Padre Island there is a convergence zone of mixed sediments from the Rio Grande and northern fluvial inputs (Hayes, 1964; McBride et al., 1996). Textural characteristics of Padre Island beach sand indicate the sand is predominately well-sorted, with a mean grain size of 2.3-2.7 ϕ (Dickinson, 1971). Petrographic analysis of sand grains by Mason and Folk (1958) along Mustang Island (approximately 30 km to the north) revealed the mineralogical composition of the sand to be 9% feldspar (about half orthoclase, half microcline), 2% chert, 3% composite metamorphic quartz and 86 % common quartz (Mason, 1958).

It is common, especially during the summer months for large amounts of Sargassum seaweed to wash up onshore, which is described by Weise (1980) to aide in the development of coppice dune fields along the foreshore (Figure 2a). From summer 2010, through summer 2011, the beach has experienced a significant accumulation of Sargassum that usually drifts from the Sargasso Sea *via* southeasterly surface ocean currents (Weise, 1980). Several types of vegetation along the backshore and foredunes help to stabilize the dunes by trapping wind-blown sand and allowing the dunes to grow over time (Figure 2b). Marshhay cordgrass (*Spartine patens*), morning-glory (*Ipomoea spp.*), and sea purslane are common on the lower parts of the dune. The middle and

upper parts of the dune are stabilized by sea oats (*Uniolapaniculata*), bitter panicum (*Panicumamarum*), and gulf croton (*Croton puncatus*). The thick vegetation cover on the back-side of the foredune primarily consists of seacoast bluestem (*Andropogonscopariuslittoralis*) (Weise, 1980).

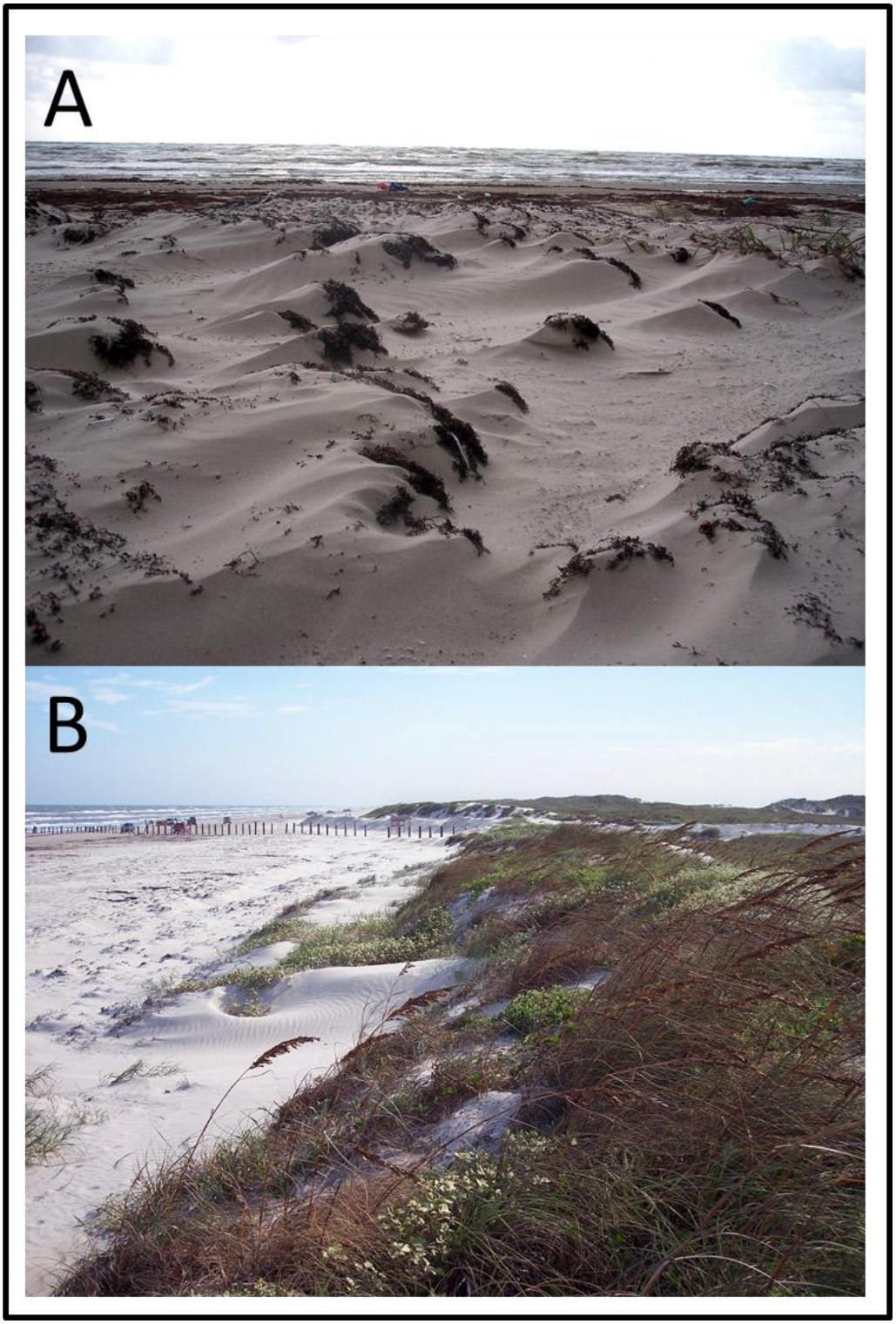

Figure 2. Example of coppice dunes along the backbeach stabilized by seaweed. (2a), and vegetated foredunes, view looking south towards South Beach (2b).

LITERATURE REVIEW

Barrier islands and spits are found along many of the coastlines of the world. These islands are important from an economic and cultural standpoint as a natural defense against coastal storms and hurricanes. Most barrier islands and spits are currently in the state of transgression (landward retreat) in response to combinations of global eustatic and local sea level change (subsidence and tectonics) and, as such, are dynamic landforms (Houser, 2009). Barrier islands typically transgress during extreme storms. When the foredunes are breached by storm surge, sediment is redistributed from the intertidal zone to the back of the dunes as washover fans and channels and/or blowout development or scarping (Davidson-Arnott, 2005; Houser, 2009; Houser et al., 2008; Sallenger, 2000). During transgression, the barrier island system will migrate landward in response to rising sea-level. The redistribution of sediment during storms and hurricanes and the rate of transgression depends on the height and alongshore extent of costal dunes relative to the elevation of storm surge(Houser et al., 2008; Morton and Sallenger, 2003; Sallenger, 2000). As a consequence, alongshore variations in the height of the dune and morphology of the beach can lead to different transgression histories and may be used to predict response and recovery of the barrier island to future storm events. In other words, over short distances along the same beach, alongshore variability of the foredunes will influence transport potential and sediment supply controlling dune growth over time.

Various conceptual models have been proposed to explain the effects of sea level rise along the coastlines of the world. Perhaps, the first and most recognizable model was proposed by Bruun in 1954 relating shoreline retreat to rising sea-level. Schwartz (1968) suggested shoreline retreat can be predicted since a typical concave-up beach profile erodes sand from the beach face and deposits it offshore to maintain a constant water depth. In other words, the redistribution of sediment resulting from rising sea level suggests that the landward displacement of the shoreline is a function of the profile slope and vertical sea level rise, assuming an ample sediment supply landward of the shoreline (Bruun, 1988; Davidson-Arnott, 2005). It has been argued that this two-dimensional model is not sufficient in explaining coastal response to a rise in sea level, because it does not take into account the influence of the foredune system (Cooper and Pilkey, 2004; Davidson-Arnott, 2005).

Davidson-Arnott (2005) proposed a different conceptual model based on the underlying assumptions stated by Bruun, but include the foredune system, which was not considered extensively. The two main differences between the Bruun model and the model proposed by Davidson-Arnott (2005) are 1) within the subaqueous area during sea level rise, the outer nearshore profile is eroded and results in a net landward sediment transfer to maintain the equilibrium profile and 2) transgression and erosion of the backshore and dune leads to a net landward transfer of sediment and landward migration of the dune. It is argued that the majority of sediment transfer occurs during storm activity. For example, Sallenger (2000) compared large and small dunes at Duck, NC, and Isles Denieres, LA, respectively, to illustrate the importance of dune height as a

barrier to storm surge. It is reasonable to expect that during a storm event, small dunes would be inundated by the surge resulting in overwash deposits, in contrast to large dunes that may not be breached at all and only scarped by the surge.

By comparing the magnitude of the storm surge compared to coastal beach-dune dimensions, Sallenger (2000) developed a useful storm impact scale that accounts for storm-induced patterns and magnitudes of net erosion and accretion along barrier islands. The parameters used for scaling the impacts of the storm are R_{HIGH}, R_{LOW}, D_{HIGH} and D_{LOW}, where R represents the high and low elevations of the landward margin of swash relative to a fixed vertical datum and D_{HIGH}/D_{LOW} represent the dune crest and dune base, respectively. From these parameters, a series of storm impact regimes can be defined by considering how R_{HIGH} and R_{LOW} vary relative to D_{HIGH} and D_{LOW}. The Sallenger (2000) impact model not only considers meteorological conditions of a given storm, but also categorizes the geologic impacts between low-lying and high-relief coastal dunes as either washover or dune-scarping, respectively.

In the four impact levels (Figure 3), Level 1 “swash regime” describes a storm where the run-up is confined to the foreshore and there is no net change in sediment transport. In the Level 2 “collision regime”, the storm run-up scours the base of the foredune ridge and results in net erosion of the dune. The Level 3 “overwash regime” designates situations where the storm surge overtops the foredune ridge as a washover and results in a net landward sediment transport responsible for island transgression. With the Level 4 “inundation regime,” the storm surge completely submerges the beach-

dune system and suggests that landward transport of sediment is much greater than during the "overwash regime."

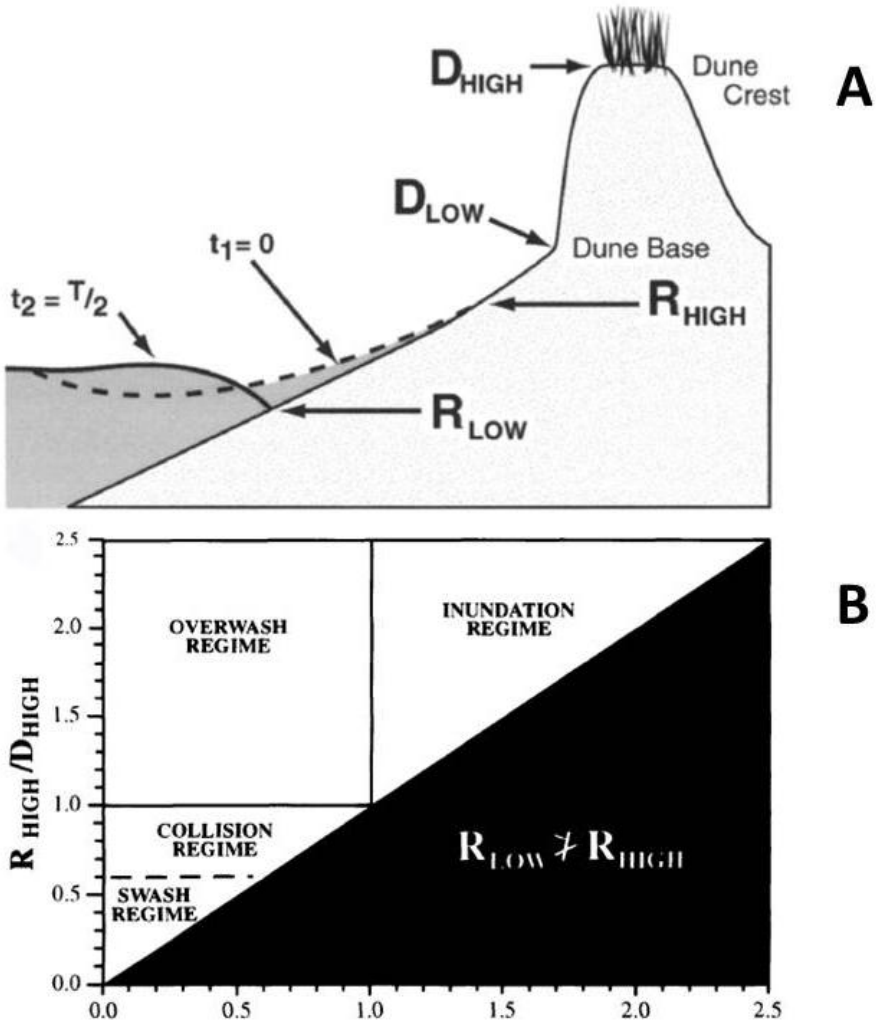

Figure 3. Schematic diagram showing variables used in the Sallenger model of storm impact on barrier islands. (a) delineation of the 4 different impact regimes along barrier islands during storm events (b) (modified after Sallenger, 2000).

Despite the usefulness of the Sallenger (2000) storm impact scale, there is a lack of information in the literature regarding how different dune heights along the same beach influence the redistribution of sediment during storms. The ability of coastal dunes

to recover and the morphological response to the next storm depends on the availability of sediment from the overwash and is only initiated when sufficient vegetation is able to trap eolian-derived sediment from the beach (Hesp, 1988; Houser et al., 2008).

Within the beach-dune system, preserved sedimentary structures can provide a relative chronology of how the dunes respond to storm activity. For example, erosional surfaces (i.e., unconformities), trough cut and fill, foreslope accretion, rearslope accretion and cross-stratification can indicate the intensity of storm impacts. GPR can be used as a non-invasive geophysical technique to investigate internal stratigraphy of the beach-dune system.

Conceptual Models of Beach-Dune Interaction

Short and Hesp (1982) suggest that the morphodynamics of the back beach and dunes are intrinsically related to the dynamics of the foreshore, and that coastal dune evolution is a function of the characteristic beach state within the dissipative/reflective continuum (Hughes, 2003; Psuty, 1988; Sherman and Lyons, 1994; Short, 1984; Short and Hesp, 1982; Wright et al., 1979; Wright and Short, 1984). For example, the gradient and width of a beach have a profound influence on the rate of potential landward eolian sediment transport and thus, dune growth over time (Short and Hesp, 1982). Dissipative beaches are comprised of a wide and generally flat backshore and beach face that allows for onshore winds to entrain and deposit fine-grained sands on the adjacent foredunes. Conversely, reflective beaches are narrow and steep with coarse-grained sands and gravel that impede dune growth over time. Intermediate beaches vary within a number of

morphologic states, depending on the modal beach state, form, and volume of available sand stored on a particular beach (Short and Hesp, 1982).

The second model, proposed by Psuty (1992), considers dune development from the perspective of sediment budget between beach and dune. This conceptual model relates sediment exchange between beach and dune to a relative budget of increasing/decreasing sediment supply. Psuty's model is fundamentally different from the Short and Hesp (1982) model in that dune development is considered a direct result of sediment budget and not necessarily a function of reflective/dissipative beach states. For example, there can be a difference between beach budget and dune budget that allows the beach-dune system to develop in opposite directions.

Psuty's model of beach-dune interaction considers two distinct components of the total system, where sediment budget for each component is measured around a set of equilibrium conditions. In this model, dune development is favored when there is a net negative sediment budget where the beach is negative and the dunes are positive. However, recent research suggests that dune growth is limited by the volume of available sediment along the backbeach, and that an ample supply of sediment from the beach to the dunes is required to allow the dunes to grow over time (Houser and Mathew, 2011). Contrary to the Psuty model, a net positive sediment budget and dune negative budget is needed for dune growth. Both existing "fixed-state" models of beach-dune interaction distinguish regional variations in dune morphology to either characteristic beach state and/or sediment budget without thoroughly explaining the processes involved (Houser, 2009).

Despite existing models and classification of beach-dune systems, there remains a barrier toward a theoretical framework that can adequately explain the synchronization between the system across spatiotemporal scales and field sites (Aagaard et al., 2004; Houser, 2009; Sherman, 1995; Sherman and Bauer, 1993; Sherman and Lyons, 1994). It has been suggested that the evolution and recovery of coastal dunes result from spatial and temporal coupling of nearshore and eolian processes (Houser, 2009).

Sediment transport between beach and dune systems has been described to be both spatially variable and temporally intermittent as a result of transport limitations across the beachface. Although process-scale studies have determined variable controls on sediment transport such as grain size, beach slope, wind and wave dynamics, there remains a limitation to predict the evolution of beach-dune systems. The important relationships between transport and supply argued by (Houser, 2009; Houser and Mathew, 2011) is consistent with both the Psuty (1992) and Short and Hesp (1982) models of beach-dune interaction, suggesting that the models are valid depending on the type of beach. It is argued that reflective beaches are transport limited, and dissipative beaches are supply limited (Houser, 2011 pers comm). However, the primary difference from previous models is that synchronization must be defined as a complex, dynamic process rather than in a fixed state and, furthermore, as a dynamic exchange of sediment between beach and dune that can account for differences in dune height and morphology for similar beach states (Houser, 2009).

One way to examine the evolution of beach-dune systems is through the use of Ground-Penetrating Radar. The GPR unit emits short pulses of electromagnetic radiation

that propagate through the substrate from a transmitting antenna and is reflected back to and detected by a receiver when the radar wave encounters distinct changes in dielectric properties in the ground (Neal, 2004). The material properties that govern the propagation of electromagnetic radiation (EMR) are dielectric permittivity (ε), electrical conductivity (σ), and magnetic permeability (μ) (Knight, 2001; Neal, 2004). EMR reflections can occur along a variety of subsurface discontinuities including changes in porosity, sediment grain shape and type, grain packing, grain orientation, and changes in moisture and salinity content. Thus, it is possible to resolve sedimentary structures and lithological boundaries(Jorgensen, 2007). The majority of reflectors from GPR surveys can be interpreted as the product of primary depositional fabric and sedimentary structures (Bailey and Bristow, 2000).

The Use of GPR in Coastal Studies

GPR is a non-invasive tool for investigating the internal structure of beach and dune stratigraphy (Bailey and Bristow, 2000; Bristow and Bailey, 2001; Bristow et al., 2000b; Buynevich et al., 2007a; Buynevich et al., 2007b; McGourty and Wilson, 2000; Neal and Roberts, 2000). For example, research by Bristow et al (1996); Clemmensen et al., (1996); Harari (1996) and others has demonstrated that GPR can image cross-stratification, erosion surfaces and the water table in coastal dunes without causing significant disturbance to the integrity of the dune (Bailey and Bristow, 2000). Studies conducted by Bailey and Bristow (2000, 2001) in Ireland and the United Kingdom show that GPR reflections can be interpreted to represent foreslope accretion; rearslope

accretion, trough cut and fill, beach and swash deposits. Results from their study along a prograding coast in Norfolk, UK suggest that dune ridge development is linked to shoreline change. Dune development is associated with coastal progradation and beach stability during calm conditions, whereas dunes are eroded during coastal storms as recorded by dune scarping (Bristow et al., 2000b). They use these data to suggest a model for coastal dune evolution that is based upon a combination of seismic interpretation techniques described by radar facies analysis and radar sequence analysis (Figure 4).

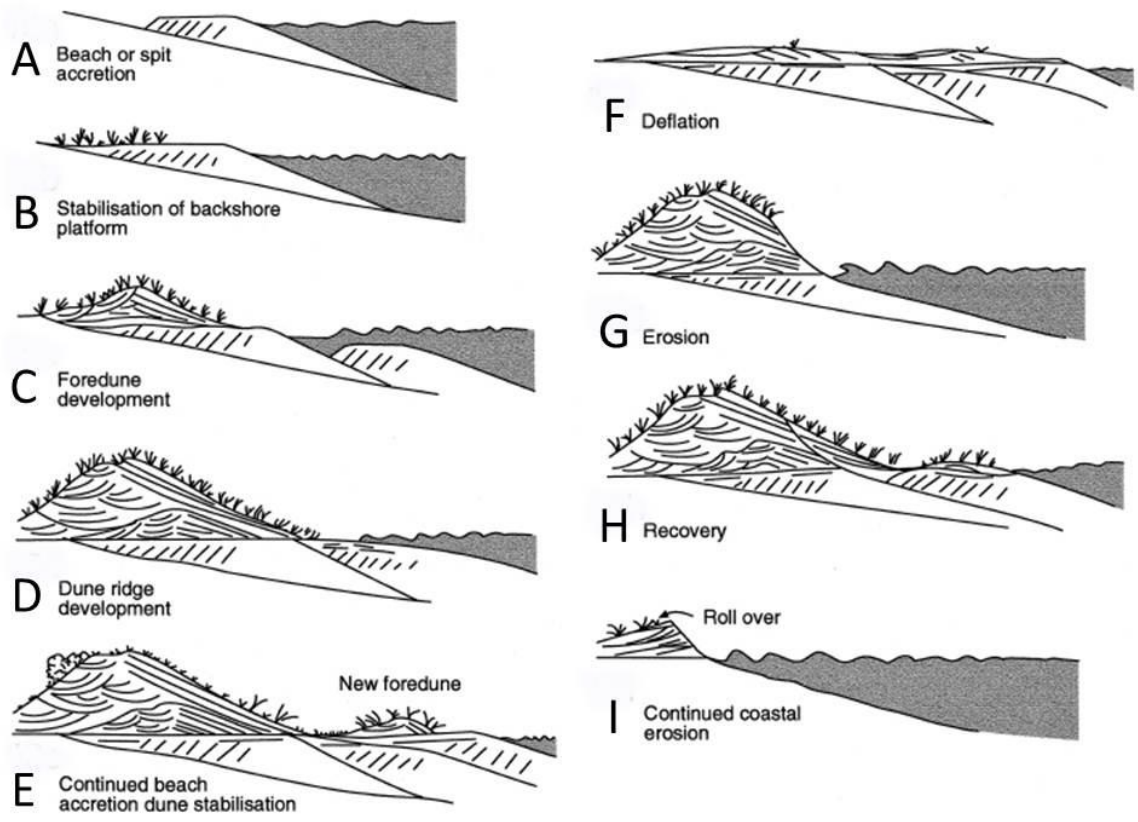

Figure 4. Dune evolution model based on GPR studies from Norfolk, UK (modified after Bristow et al., 2000).

In addition to seismic interpretation techniques, two methodologies have been proposed for the interpretation of GPR profiles; radar facies analysis and radar sequence analysis (Bristow et al., 2000b). Radar facies are repeated packages of reflections with similar character and geometry, and radar sequence boundaries are located at reflector terminations. Because there are typically a large number of GPR reflector terminations accompanying small-scale sedimentary structures, only the more extensive terminations are identified as sequence boundaries (Bristow, 1995).

From their GPR surveys of coastal dunes, Bailey and Bristow (2000) identify seven different radar facies based on the continuity, dip angle, shape and orientation of the GPR reflections (Figure 5). For example, discontinuous low-angle (< 20°) clinoforms with seaward dips are interpreted to represent foreslope accretion. Structures located below the imaged water table are interpreted as marine sediments, whereas feature above the water table are interpreted as eolian sediments.

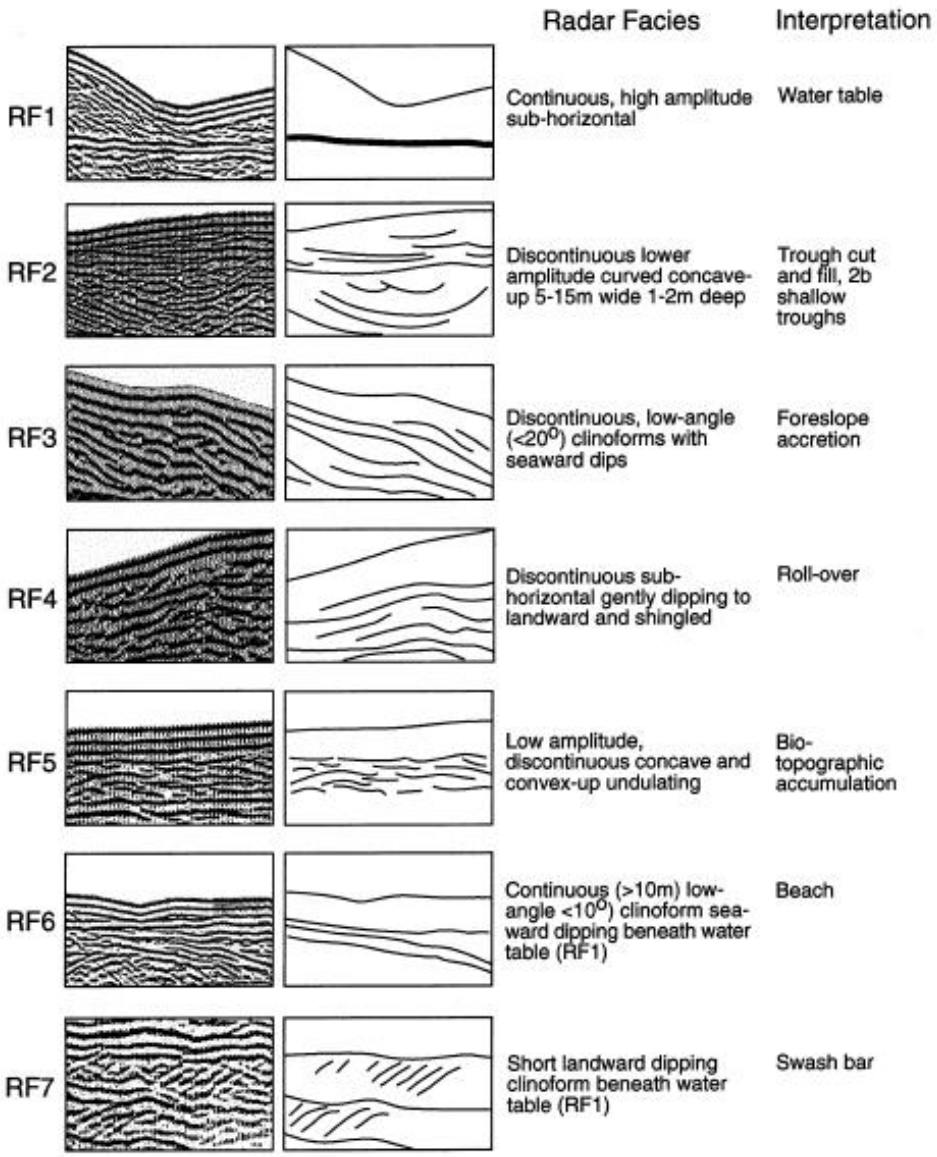

Figure 5. Radar facies (Modified from Bristow et al., 2000).

An example of an interpreted GPR profile from a parabolic dune ridge in Abberffraw, North Wales, illustrates the complexity of beach-dune systems (Figure 6). The most prominent feature is the horizontal, laterally continuous reflector that is interpreted to represent the top of the water table. By determining the locations of reflector terminations, radar sequence-boundaries and facies are described and provide the basis for interpreting the history of the beach-dune system. Bristow et al., (2000b) describe landward-dipping reflectors representing rearslope accretion from eolian-derived sand, directed by prevailing winds. Trough-cut and fill structures are created particularly on the crest of the dune from erosion and deposition of wind-blown sand. The separation between older and younger packages of rearslope accretion suggests "roll-over" of the dune system as it evolves through time. The term "roll-over" is analogous to transgression in that the entire coastal profile migrates landward in response to a rise in sea-level. Although these results may explain dune evolution along beaches in the UK, they may or may not translate across field sites.

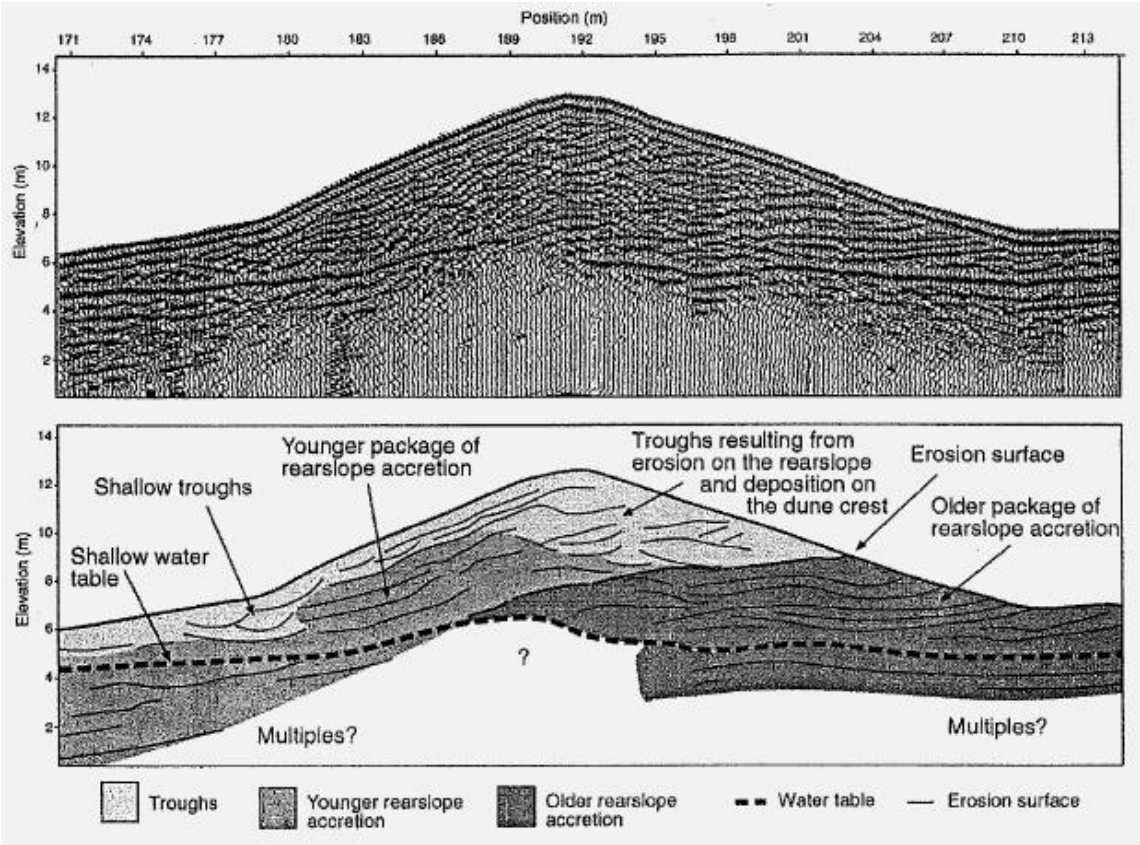

Figure 6. Detailed structure of a parabolic dune ridge at Abberffraw, North Wales (modified after Bristow and Bailey, 2001)

Despite the usefulness of GPR as a non-invasive technique to investigate internal structures of various-sized dunes, there are inherent limitations that must be taken into account. For example, interference between antennae by direct ground and air waves prohibit the upper meter of the GPR profiles to be interpreted. Additionally, the "range-resolution tradeoff" described by Davis and Annan (1989) limits the degree of vertical resolution that can be obtained. With higher-resolution antennae, it is possible to resolve sedimentary structures at a finer-scale (i.e., cm scales), but some researchers argue that

the only way to accurately describe and interpret sedimentary structures is by trenching and/or coring.

Vibra-Coring in Coastal Environments

The usefulness of GPR for investigating sedimentary structures in a variety of environments has been demonstrated in great detail (Bailey and Bristow, 2000; Bristow, 1995; Bristow et al., 1996; Bristow and Bailey, 2001; Bristow et al., 2000b; Bristow et al., 2005; Buynevich et al., 2007a; Garrison et al., 2010; Jol and Bristow, 2003; Jorgensen, 2007; McGourty and Wilson, 2000; Neal, 2004; Neal and Roberts, 2000; Sassen and Everett, 2009; Sassen et al., 2009). Validating GPR data with corresponding outcrops, trenches and/or coring has given researchers the ability to correlate GPR reflectors with structural features. As noted changes in grain size, grain packing, orientation, porosity, moisture and salinity content and other physical properties directly affect the properties of radar wave propagation through the medium. The radar reflections influenced by these changes in physical properties can be interpreted to represent actual sedimentary structures. Prior to recent advances in GPR technology, trenches and cores were excavated to view and study the stratigraphy of depositional systems, including coastal environments. From trenches and cores, samples can be collected and processed for grain size analysis in addition to a variety of physical, chemical and biological testing techniques.

Vibra-coring is a technique that has been widely used in a variety of environments for collecting core samples of unconsolidated sediments(Schwartz, 2005;

Schwartz and Birkemeier, 2004). The vibrating mechanism of a vibra-core sometimes called the “vibra-head” or “drill head” operates on hydraulic, pneumatic, mechanical or electrical power from an external source. Attached to the drill head is a core barrel or tube that is driven into the underlying substrate by the force of gravity and enhanced by vibration energy when the motor is operational. Once the core barrel is fully inserted into the ground, the motor is turned off, and the core is extracted by a wench and pulley system.

One of the advantages of using a vibra-coring device is that the system is relatively light and versatile and can be transported to numerous sites in a relatively short timeframe. Some vibra-core systems, such as the WINK Vibra-core Drill™ allow the attachment of additional sections of core barrel, enabling cores to be extracted from depths of tens of meters. Other advantages using vibra-cores instead of conventional methods, such as hammer-coring, involve how energy is transferred through the sediment. In vibra-coring, high-frequency vibrations transfer more energy to the sediment, which reduces wall friction inside and outside of the tube. In other words, only a small rind around the outer diameter of the core that is in contact with the core liner is disturbed meaning that the inner core remains intact.

Following coring activities, the cores can be analyzed and sub-sampled either on site or in a laboratory. In addition to core descriptions, samples collected for grain size analysis can provide valuable information regarding sediment transport and the processes involved to categorize beach vs. dune environments.

Grain Size Measures

Grain size analysis has been widely used to categorize sedimentary environments and to determine the processes by which they formed(Boggs, 2001). The ability for sediments to be transported by wind or waves is greatly influenced by the size of the particles. The larger the size, the more energy is required to entrain the particle. Thus, grain size measures can provide insight regarding the degree of hydrodynamic and aerodynamic conditions for a given depositional environment (Inman, 1949). There are various techniques used to determine grain size distribution including wet sieving, dry sieving, settling tubes, measurement by laser granulometers, and others. However, all of the techniques involve dividing the sample into a number of size fractions which enables a grain size distribution to be determined from the weight or volume percentage for each fraction compared to the entire sample (Blott and Pye, 2001).

Measuring grain size distributions for sediment samples is usually described by its deviation from an ideal statistical distribution. A variety of statistical measures have been developed to classify sediments based on their textural properties (Folk and Ward, 1957; Inman, 1952; Krumbein, 1938; McCammon, 1962; Otto, 1939; Trask, 1932). The four grain size parameters commonly used in grain size analysis are mean size, standard deviation (i.e., sorting), skewness and kurtosis, which can be calculated using a variety of equations (Folk, 1966).

The mean is a first order approximation of the magnitude of forces by wind or water and reflects the overall average sediment size. For the scope of this paper, the following formulae follow the Folk and Ward (1957) logarithmic graphical measures

method. The mean is determined by the following: where $\phi 16$ represents the 16th percentile, $\phi 50$ is the 50th percentile and $\phi 84$ is the 84th percentile of the distribution in phi units.

$$\mu = \frac{\phi 16 + \phi 50 + \phi 84}{3} \tag{1}$$

The standard deviation indicates the range of sizes for a given sample and, therefore, is analogous to sorting. A well-sorted sample, having a small standard deviation value is indicative of sediment transport. For coastal environments, poorly sorted sands are indicative of beach deposits whereas well-sorted sands by wind are commonly found in dune environments. Sorting is determined by the following:

$$\sigma = \frac{\phi 84 - \phi 16}{4} + \frac{\phi 95 - \phi 5}{6.6} \tag{2}$$

where, the various percentiles are used. Skewness is a measure of symmetry for the distribution within a sample. A positively skewed sample indicates the addition of fine grains by wind or removal of coarse grains by water. The skewness of a sample is calculated by the following:

$$Sk = \frac{\phi 16 + \phi 84 - 2\phi 50}{2(\phi 84 - \phi 16)} + \frac{\phi 5 + \phi 95 - 2\phi 50}{2(\phi 95 - \phi 5)} \tag{3}$$

where, the various percentiles are used. Kurtosis measures the normality of a distribution as a ratio between the sorting in the central part of the curve with the sorting of the tails. If the central part of the curve is well sorted, then the curve is called Leptokurtic. Conversely, the curve is termed Platykurtic if the tails are better sorted than the central portion. The formula used for kurtosis is:

$$K = \frac{\phi 95 - \phi 5}{2.44x(\phi 75 - \phi 25)} \quad (4)$$

where, the various percentiles are used. GRADISTAT™ was used to calculate grain size statistics for multiple methods.

Determination of Beach and Dune Environments from Grain Size Analysis

Changes in grain size influence the amount of shear stress required to initiate and sustain the movement of sedimentary particles. Factors that influence grain size distribution for coastal sediments include sediment source, distance from the sediment source, distance from the shoreline, topography, and the transport mechanisms (Abuodha, 2003). The extent of wave and wind energy across the beach-dune system and sediment size are major factors in determining morphodynamic processes across the littoral zone (Chauhan, 1992). Thus, through the use of grain size analysis it is possible to distinguish beach and dune environments by comparing the four grain size parameters.

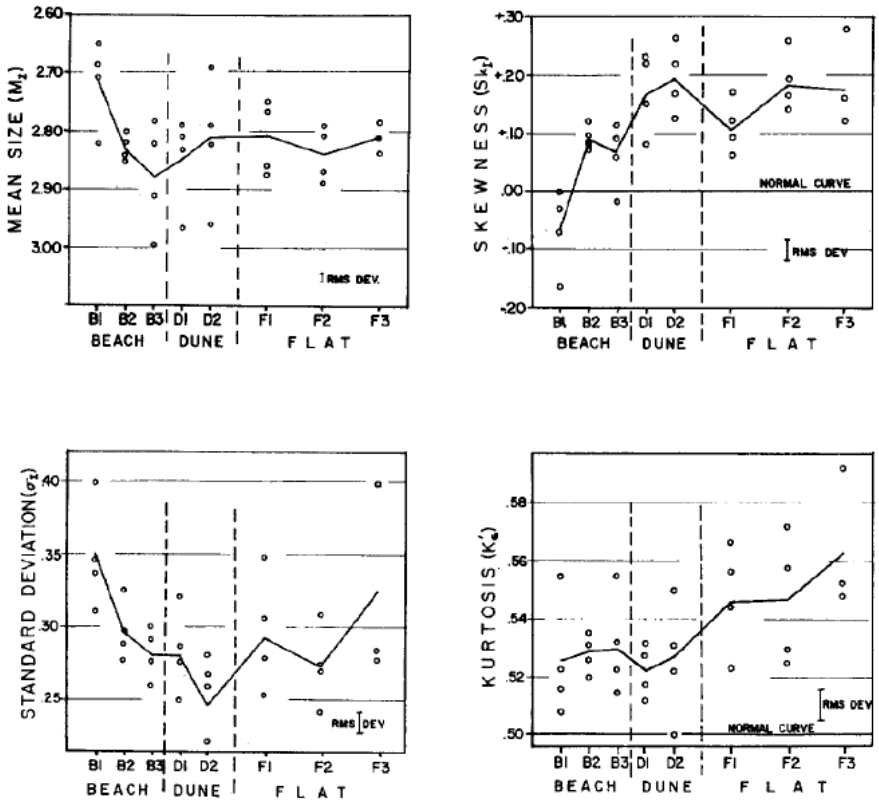

Figure 7. Detailed plots of grain size parameters along Mustang Island, TX. Circles represent one of four crosswise traverses across the island (Modified from Mason and Folk, 1958).

Mason and Folk (1958) compared grain size parameters from beach, dune and eolian flat environments, respectively along a 25 km traverse of Mustang Island, TX (Figure 7). Prior to their study, mean grain size and sorting were the two most commonly used parameters to distinguish geologic processes for a particular environment. However, along Mustang Island the source sediment from the Colorado River exhibited an extremely uniform grain size and was exceptionally well-sorted. Results from their study suggest that subtle variations in sediment transport have a marked influence in the distribution of the tails of the statistical distribution. In other words, skewness and

kurtosis measures the sorting of the tails of the grain size distribution and these values significantly change with the addition or removal of small amounts of sand. Kurtosis values are normalized using the following equation (From Mason and Folk, 1958):

$$K_G' = \frac{K_G}{K_G + 1} \tag{5}$$

Figure 8 demonstrates the usefulness of plotting skewness and kurtosis for distinguishing the three environments for Mustang Island. Folk (1966) further explains that the beach samples were negatively-skewed from the addition of a small tail of coarse grains, whereas the dune and eolian flat samples were positively-skewed by the addition of silt that moved the tail out. Mason and Folk (1958) suggest that as sediment is transported cross-shore into the dunes, the coarse fraction of the size distribution lags behind through progressive sorting as the eolian transport potential (i.e., energy) decreases resulting in a well-sorted, positively skewed distribution within the dunes. The importance of grain size analysis as a tool to classify depositional environments remains one of the primary ways to understand the processes that govern the evolution of these systems over time.

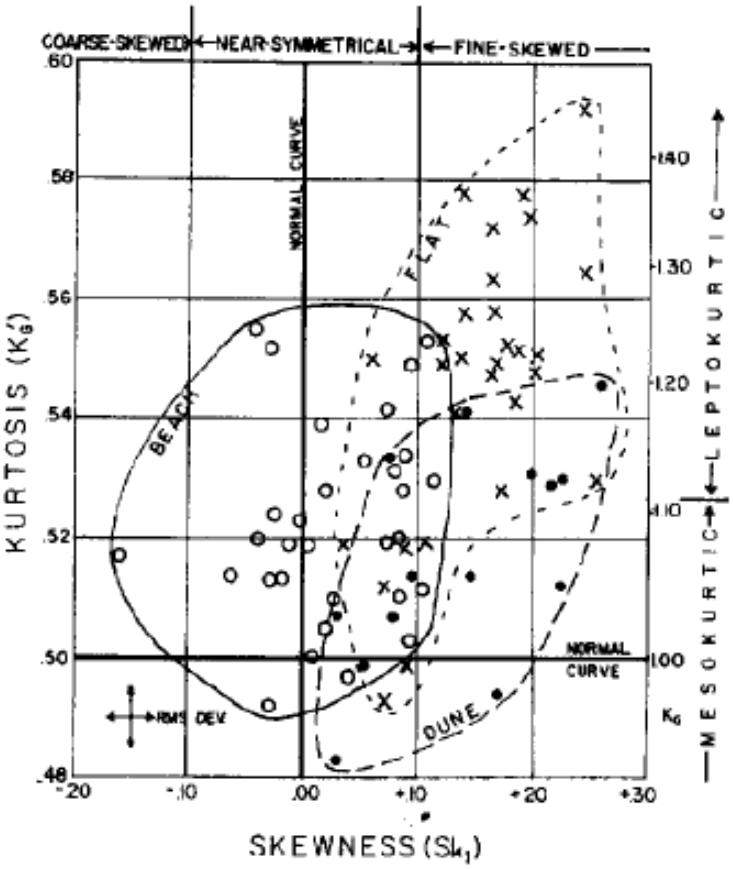

Figure 8. Scatterplot showing skewness vs. kurtosis distinguishing the three types of environments. The open circles are beach samples, closed circles are dune samples, and crosses are eolian flat samples (modified from Mason and Folk, 1958).

Geochemical Characterization of Coastal Sediments

The geochemical composition of sediment is a function of grain size and a number of formation processes such as; weathering, sorting, decomposition and others (Von Eynatten and Tolosana-Delgado, 2011). Various non-destructive methods have been employed to measure changes in physical sediment properties from a number of depositional environments. Changes in porosity, bulk density, and permeability provide a first-order assessment of the sediment, which facilitates accurate stratigraphic

interpretation. However, measuring changes in the chemical composition of sediments remained a challenge for many years.

X-ray fluorescence (XRF) logging was first developed in the Netherlands in 1988 and revolutionized non-destructive core logging by measuring changes in chemical composition (i.e., major, minor and trace elements) downcore (Richter et al., 2006). The application of XRF scanning includes initial correlation between cores, preliminary stratigraphic interpretations, investigating provenance of terrigenous material, tracing early diagenesis and recognition of sedimentological events from specific lithological changes (Richter et al., 2006).

X-ray fluorescence (XRF) uses X-ray radiation by exciting electrons from an inner shell of an atom. The electron is ejected from the inner shell, resulting in a vacancy that is subsequently filled by an electron falling back from an outer shell. The energy difference between both shells emits a characteristic electromagnetic radiation wavelength that is specific for each element. The amplitudes of the peaks in the XRF spectrum are detected by an X-ray optical system and recorded as peak areas, or counts for a range of elements. The response depth of each element to incoming X-ray radiation is governed by the wavelength of the emitted radiation and related to the atomic weight and chemical composition of the sample. Different energies are required for the detection of light, heavy and trace elements. For example the major elements including; Al, Si, P, S, Cl, K, Ca, Ti, Mn, Fe, Cu, and Zn can be detected by the XRF scanner using 10kV energy (Richter et al., 2006).

The use of XRF in coastal environments has only recently been explored in detail. As a result, there remains a lack of information regarding the utility of XRF scanning of coastal sediments. A few studies have investigated the relationships between grain size, textural properties and geochemical composition of sediments (Alagarsamy and Zhang, 2010; Leoni et al., 1991; Richter et al., 2006; Von Eynatten and Tolosana-Delgado, 2011; Yang et al., 2004). For example, Leoni et al. (1991) suggest that distribution of major elements depend on grain size and the mineralogical composition surficial sediments from a study conducted in the northern Tyrrhenian Sea. They further explain that calcium concentrations are exclusively correlated with carbonates and mostly concentrate within coarser grades of sediment that are frequently comprised of calcareous shell debris.

METHODS

The typical range of frequencies for GPR vary between 10-1000 MHz in the microwave band of the radio spectrum (Jol and Bristow, 2003). For this study, the 200 MHz antennae were chosen for high-resolution imaging of the beach-dune system. Shorter wavelength antennae provide higher vertical resolution at the expense of greater depth penetration through the medium (Davis and Annan, 1989; Sharma, 1997). The depth of penetration for the three sites ranged from approximately 4-5 m. For the beach-dune system, the depth of penetration is greatly influenced by the location of the water table. As moisture and/or salinity increases the radar signal is attenuated. However, it is possible to resolve structures below the water table (Bristow and Bailey, 2001).

The vertical resolution for a given GPR survey is a function of the wavelength of the antennae and the velocity of the radar wave through the underlying substrate. To determine the appropriate velocity (m ns^{-1}) a common mid-point (CMP) gather was conducted. The calculated velocities from CMP surveys range from 0.11-0.13 m ns^{-1}, which are typical values for slightly damp sand. An average velocity of 0.12 m ns^{-1} was used when migrating data for all the profiles in this study. Commonly quoted velocities for dry sand range from 0.1-0.2 mns^{-1} and values for wet sand are 0.05-0.08 mns^{-1}(Neal and Roberts, 2000). The radar wave velocity (v) is a function of relative permittivity (ε_r) and magnetic permeability (μ_r) and is given by the formula (Davis and Annan, 1989):

$$v = \frac{c}{\sqrt{(\mu_r \varepsilon_r)}} \tag{6}$$

where,c is the speed of light ($3x10^8$ m s^{-1}), $\mu_r = \left(\frac{\mu}{\mu_0}\right)$ is the magnetic permeability of the medium, and $\varepsilon_r = \left(\frac{\varepsilon}{\varepsilon_0}\right)$ is the relative permittivity of the medium. For most geologic materials μ_r = 1, with the exception of highly magnetic rocks. Therefore, ε_r can be considered the controlling factor for calculating radar velocity. For this study a ε_r value of 9 was used as an average value for dry sand, which yields a radar wave velocity of 10^8 m s^{-1}. The vertical resolution was obtained by calculating the wavelength (λ), which is governed by frequency and velocity:

$$\lambda = \frac{v_1}{f} \tag{7}$$

where, f is the antennae frequency. With an average radar wave velocity of 10^8 m s^{-1} and a nominal frequency of 200 MHz ($2x10^8$ Hz), the calculated wavelength is 0.5 m. Given that the maximum resolution achievable cannot be greater than λ/4, the estimated vertical resolution is approximately 12.5 cm for a velocity of 0.12 mns^{-1} used in this study (Sharma, 1997). This implies that individual laminae cannot be determined and interpreted from the GPR profiles. However, packages, or sets of sedimentary structures >12.5 cm can be resolved and interpreted from the profiles (Bristow et al., 2000b). Reflector terminations may indicate pinch-outs and/or individual surfaces and are sometime seen in the GPR data as “bright spots.” Previous studies by Bristow, Bailey and others show that bedding planes in coastal and eolian dunes are usually continuous

for several meters. Therefore, a step-size of 0.25 m used in this study should be adequate to resolve most sedimentary structures.

GPR Data Acquisition

The GPR profiles were collected using a Sensors and Software PulseEKKO PE100® system with 200 MHz antennae using standard methods (Bailey and Bristow, 2000; Bristow and Bailey, 2001; Bristow et al., 2000b; Knight, 2001; Neal, 2004; Neal and Roberts, 2000). A total of four transects were conducted at each site. The main transect and two shorter transects (one to the north and one to the south) were oriented perpendicular to the dune. Additionally, dune-parallel transects were collected at each site along the beach-dune interface. For all transects, the antennae were oriented parallel to the dune in broad-side reflection mode and were spaced 0.5 m apart. A step size of 0.25 m was chosen with a stack of 32 measurements at each trace. Additional system parameters were set for a time window of 100 ns and a sampling interval of 100 ps, which resulted in 1000 points per trace. The operating mode was set to step, which means that each trace was manually triggered by the operator at each 0.25 m spacing and repeated for each point for the entire length of the transect. The antennae were pressed as close to the ground as possible (when encountering vegetation) to minimize ground-air coupling. It is important to note that the upper meter of each profile is not interpretable because of interference between the transmitter and receiver. Of all the profiles, the depth of penetration was the greatest at the large dune, which is likely a result of setting a greater time window during data acquisition.

The beach profiles were recorded using a Topcon 230W Electronic Total Station™ using standard methods (Figure 9). Measurements were taken at approximately 0.5-1 m spacing's, where higher-resolution was recorded in areas with abrupt changes in elevation, particularly across the dunes. To supplement the GPR and beach profile data, each site was photographed and scanned with a Trimble GX 3-D™ ground-based LiDAR system (Figure 9). The scans provided a three-dimensional view of the beach-dune transition and were set at a 15 mm sampling interval. In addition to ground-based LiDAR scans, the elevations of the start and end of each transect were geo-referenced from LiDAR data taken in December, 2010 by the National Park Service, one month prior to the GPR surveys (Table 1). At the conclusion of each site survey, a hand-held GPS was used to record the exact location of the beginning and end of each transect and the top of the dune for repeatability.

Table 1. Geo-referenced LiDAR elevations from the start and end of the main profile and GPR transect at each site. (Courtesy of the National Park Service, December 2010).

	Small Dune	Intermediate Dune	Large Dune
Starting Elevation (m)	0.53	0.80	0.94
Ending Elevation (m)	1.83	1.91	1.66

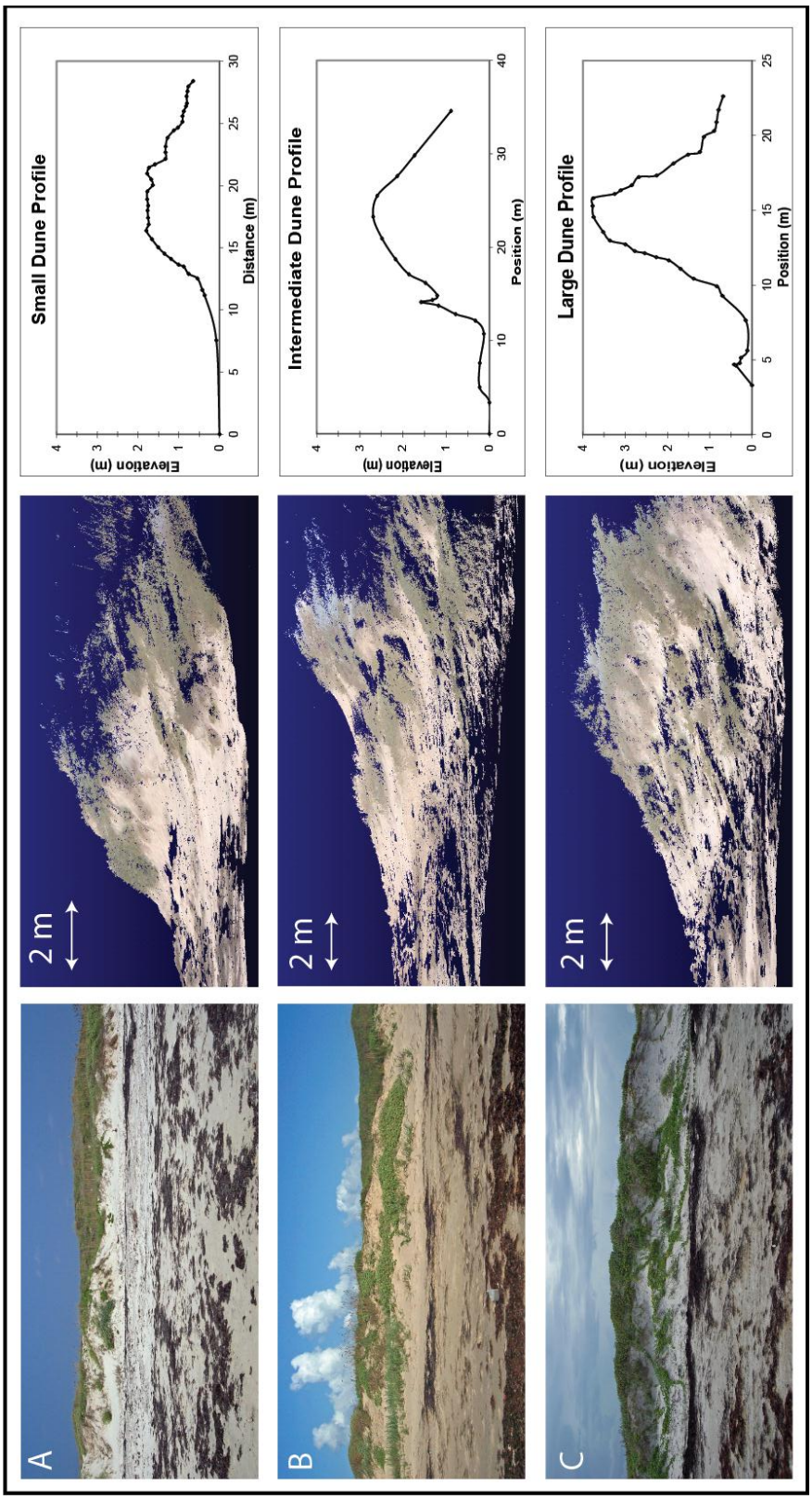

Figure 9. Photographs, ground-based LiDAR scans and total station profiles for all three sites. Small dune (A), Intermediate dune (B), and Large Dune (C).

Processing of GPR Data

The data was processed using EKKO_View Deluxe® and EKKO_View V 2.0® visualization software developed by Sensors and Software. Minimal processing was applied to ensure accurate data. During data acquisition, several blank-traces were recorded that resulted from signal problems (time zero offset) or interference from radio waves, cell phones etc. Therefore, the first step for data processing was to remove the blank-traces with the "Delete Traces" function. After the blank traces are deleted, the remaining traces are renumbered and repositioned so the total length of the profile is correct. Subsequently, three filters were applied to the data (Figure 10) and included Dewow, Background Subtraction (21 traces) and Automatic Gain Control (AGC) (window width = 1.5, maximum gain = 250).

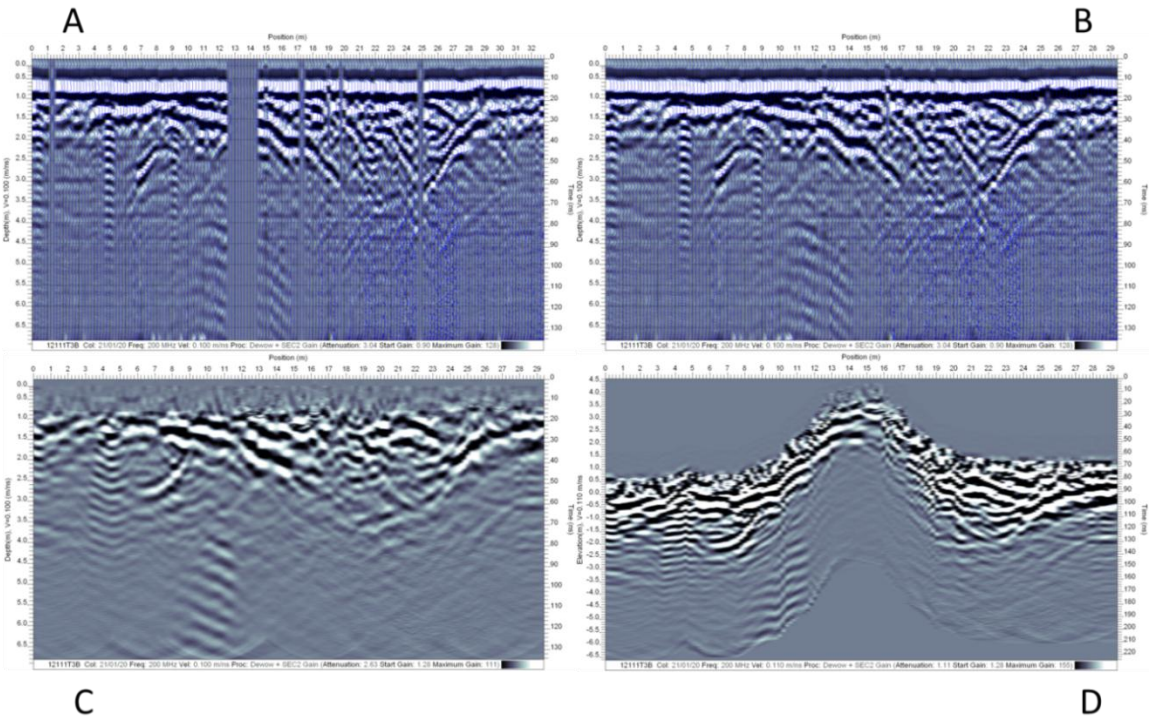

Figure 10. GPR processing steps. A). Remove blank traces. B). Blank traces removed. C). Dewow, Background subtraction (21 traces), Migration (0.12 m ns^{-1}). D). Topographic correction and non-permanent AGC filter (maximum gain = 250) applied.

The Dewow function removes unwanted low-frequency signals and preserves high-frequency signals that depend on the placement of antennae and electrical properties of the ground. The Background Subtraction applies an average background subtraction to the data set, where each trace is replaced by the original trace minus the average trace within the window centered on the original trace. The AGC Gain Control equalizes all signals by applying a gain which is inversely proportional to the signal strength and is useful for defining reflecting events. The data was migrated using an average value of 0.12 m ns^{-1} that was obtained from common mid-point (CMP) analysis. Data Migration applies an artificial image reconstruction process to the data set and

focuses scattered signals to point targets from hyperbolic responses (Sensors&Software, 2001). It is important to note that the underlying sand has varying degrees of moisture content, where the surface sands are dryer than the sand at depth. The heterogeneity in moisture content implies that the radar wave velocity changes with depth. Therefore, more than one velocity should be used when migrating the radar files otherwise some of the data may be under or over-processed, appearing as hyperbolas within the profile. A trench was excavated in close proximity to the large dune and revealed a sediment-water interface at a depth of 130 cm. Assuming a similar water depth for all three sites, the most significant contrast in radar wave velocity should occur at this horizon. Because the upper 1 m of all the profiles is not interpretable (i.e., interference between antennae), one velocity was used with the assumption that the reflectors are properly migrated. All the radar files for each of the three sites were processed in the exact same way for consistency.

After all the filters were applied, the radar files were corrected for topography. EKKO_View Deluxe requires a special .top file extension (ASCII file) containing topographic data measured by the Total Station. Each topographic file contains (XYZ) coordinates that were corrected by applying a statistical “sum of squares” calculation for the position (XY) component of the data while the vertical (Z) values were referenced to mean sea-level (0 m). For each GPR profile, the corresponding topographic data was imported and shifted to permanently move traces up or down to reflect the true stratigraphic context of the radar profile.

Vibra-coring

Following preliminary GPR data processing and interpretation, it was realized that the upper meter of the radar profile was not interpretable. Depending on the placement of the antennae, there will inherently be interference between the transmitter and the receiver that will produce noise at the upper-surface of the radar profile. In order to account for the missing information from the GPR data, a series of vibra-cores were collected at each site.

The vibra-cores were taken using a WINK Vibra-core System™. Each core was approximately 1.5 meters in length, which accounts for the gap in coverage from the upper meter of the GPR profiles. At each of the three sites, a core was taken at the start of the GPR transect located along the backbeach. A second core was taken at the beach-dune interface and a third core was taken on top of the dune or on the back-side of the dune, depending of the amount of vegetation cover. Four cores were extracted at the small dune site from the backbeach, beach-dune interface, top of the dune and on the backdune. Three cores were extracted from the intermediate dune site from the backbeach, beach-dune interface and top of the dune. Five cores were extracted from the large dune site. Two cores were collected from the backbeach, two from the beach-dune interface and one from the backdune. The coring system was modified to accommodate a 3 inch-diameter (7.62 cm) PVC core liner and orientation lines were drawn normal to the dune (Figure 11). A total of twelve vibra-cores were collected along the three main GPR transects at each site. Following extraction, the core-liners were capped at both

ends and transported to the Gulf Coast Repository (GCR) at the Integrated Ocean Drilling Program (IODP) facility at Texas A&M University for further analysis.

Figure 11. Modified vibra-coring system accommodating 3-inch-diameter PVC pipe.

Core Processing and XRF Analysis

The cores were stored at the GCR refrigerated core repository at a temperature of 40°F to reduce biologic decomposition and to prevent dehydration. At the GCR, a simple jig was assembled to securely hold the cores while splitting. The cores were split along the orientation lines marked in the field so that the split core revealed a cross-sectional view of sedimentary structures oriented perpendicular to the dunes. Each PVC core liner was cut with a circular saw and split into working and archive halves with a fishing line. Immediately after splitting, the cores were scanned using a Digital Imaging System

(DIS) provided by IODP. High-resolution images were taken for each of the archive halves. The archive halves were scanned on an Avaatech XRF Core Scanner™ for elemental analysis. The settings used for the XRF core scanner are as follows: 10kV energy, 0.5 mAmp at 30 second scan-time using no filter and scanned at 1 cm resolution along the length of each core. Within the 10kV spectrum, the lighter (main elements) were recorded as counts vs. depth and include Al, Si, P, S, Cl, Ar, K, Ca and Ti. Some intervals were not scanned if there was a void space, if the surface was depressed or if sharp objects such as large shells posed a risk of damaging the X-ray optical system. The working halves were sub-sampled with 10 cc plugs every 10 cm along the core for sieving and grain size analysis. The archive half from Site 2-D "back-dune" was also sampled because the other half was compromised during splitting.

Grain Size Analysis

Samples were washed in a U.S. Standard # 200 sieve (75 μ) to help remove excess organic material and sediment finer than 3.75 ϕ. The samples were then dried in an oven at 100°F for at least six hours, cooled to room temperature and organized into sample bags that weighed on average 25 g. Each sample was sieved using an ATM Sonic Sifter© for one minute. A total of 146 samples were sieved. Grain size fractions ranged from U.S Standard # 3.5 – 230 sieves (-1.5 to 4 ϕ). The weight of each fraction was recorded and the results from all the samples were imported into GRADISTAT™ to calculate grain size statistics.

GPR RESULTS

A series of GPR profiles were collected to capture the variation in beach-dune morphology and to determine whether there are significant structural differences between large, intermediate and small dunes. Site locations were chosen along transitions between dissipative and intermediate beach states (i.e., beach width) and the position of offshore bars (Figure 1). Following the Sallenger (2000) storm impact model for a given storm surge, the small dune is defined by low-lying topography that is the most susceptible to overwash. The large dune is the highest dune within the study area that typifies the collision regime. The intermediate dune represents a transition between overwash and collision regimes, with the underlying assumption that all three dunes are impacted by the same level of surge, during the same storm.

The smallest dune is located in an area where the beach-width is between the width of the large and intermediate dune sites and the distance of the offshore bars is between the large and intermediate bar distances. The intermediate dune is located at the widest part of the beach, where the distance between the offshore bars is the greatest. The large dune is located where the beach is the narrowest and the offshore bars are closest to the beach.

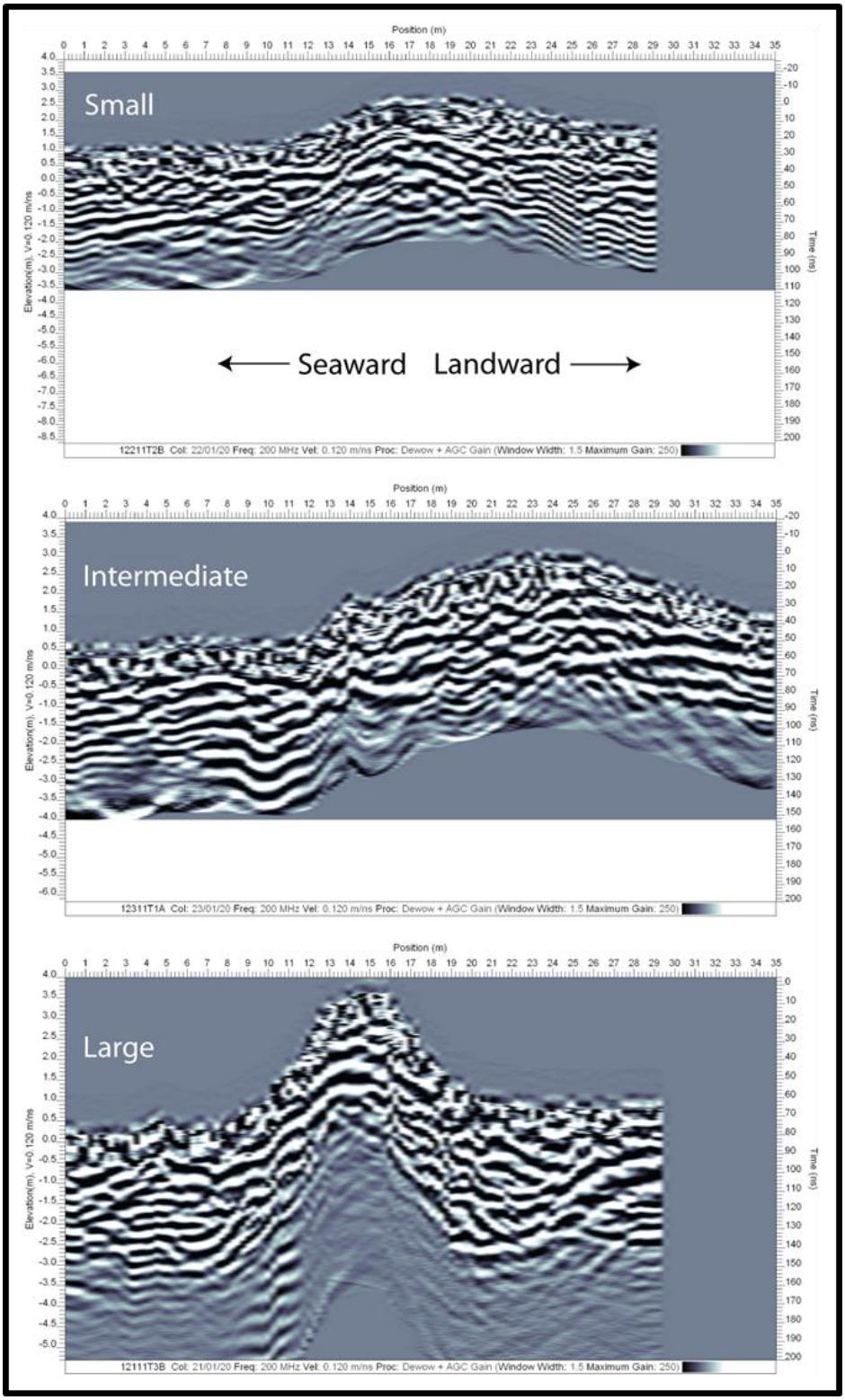

Figure 12). Site 1-3 GPR profile comparisons at the same vertical and horizontal scale.

A sequence of four GPR transects were collected at each of the three sites. The main transects (i.e., T1A, T2A, T3A) were the longest at each site and ranged from 29.5-34.75 m in length (Figure 12). The shorter, dune-normal profiles were offset either 5 or 10 m to the south and north of the main transect and ranged from 17-33 m in length. The south profiles were designated T1B, T2B and T3B and the north profiles as T1C, T2C and T3C respectively. At each site, dune-parallel transects were also surveyed and designated T1D, T2D, and T3D and ranged from 16-30 m in length. The total distance between the intermediate dune and large dune sites is 2.5 km. A general configuration of the GPR surveys is given in Figure 13. Figures 7-9 are presented using the same scale to place the dimensions of the dunes into proper context. The following sections present the results of each survey in greater detail.

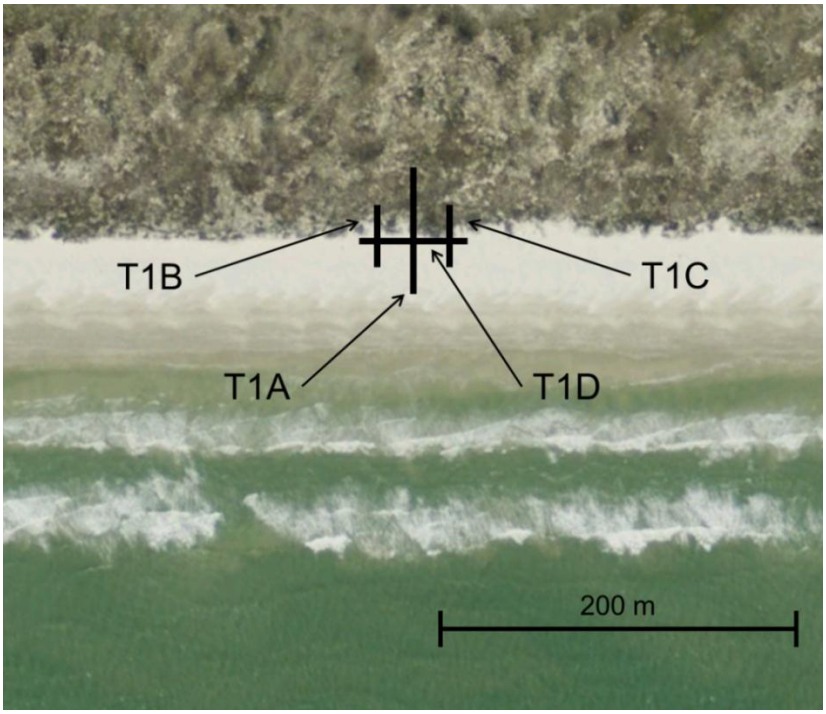

Figure 13. Configuration of the GPR transects used at each site (Image taken from Google Earth™ 2010).

Small Dune GPR Profiles

The main GPR profile at Site 2 (27° 25’ 43.8” N, 97° 17’ 44.8” W) is located at the southern end of the Malaquite Beach Campground. The profile starts at the backbeach, beyond the influence of the highest spring-tide, where the surface moisture decreases and is marked by wrack-line debris from storm activity. The small dune has a maximum height of 1.79 m and has nearly no vegetation cover until the crest of the dune. The main profile (T2A) is surrounded by larger dunes to the north and south (a few meters on either side) and is considered a transition zone between the intermediate-sized dunes. The low-lying topography and marginal vegetation cover has allowed the dune to develop a small blowout (Figure 14). In contrast to the other two sites, this dune does not have a well-developed berm. The dune is approximately 15 m wide.

At the start of the profile, from 0-10 m, there are low-angle seaward dipping reflectors that persist to a depth of 3.5 m (Figure 15). At the beach-dune interface (12 m), there is a transition from steep, seaward-dipping reflectors to more gradual landward-dipping reflectors on the back-side of the dune centered roughly at the dune crest. The reflectors on the backdune (20-29.5 m) are low-angle, gently landward-dipping and are stacked. Within the core complex of the dune, the reflectors become more horizontal with depth. Closer to the surface, there seems to be a general lack of structure and therefore is difficult to distinguish individual features.

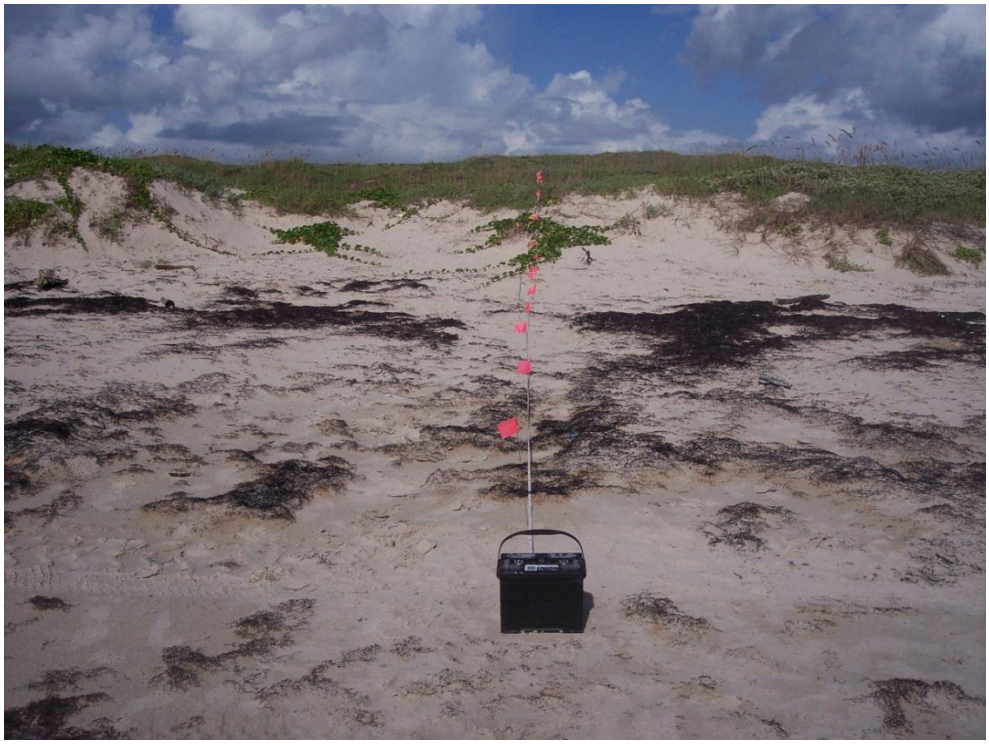

Figure 14. Small dune location, showing main GPR transect (T2A) and small blowout.

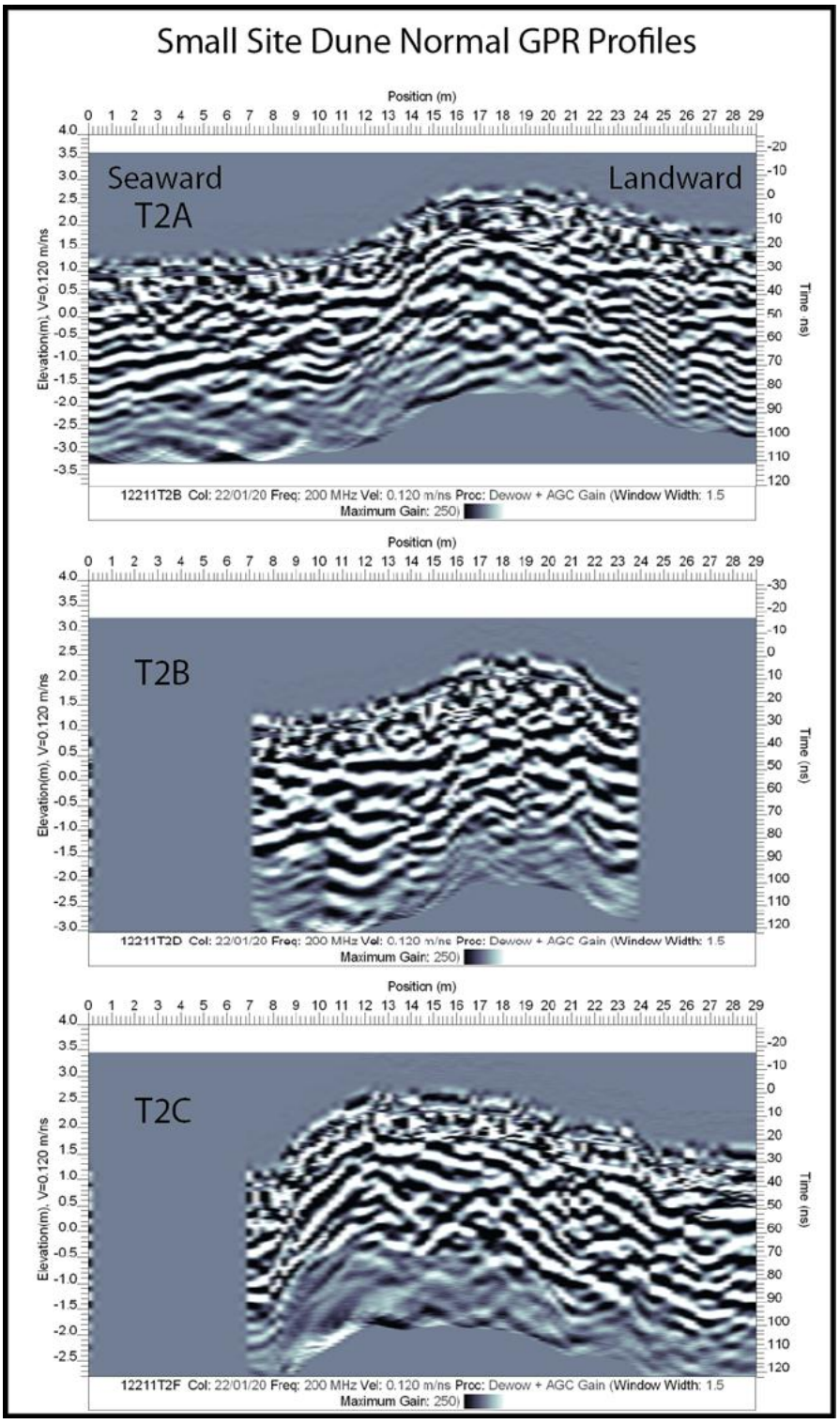

Figure 15. Small dune normal GPR profiles; main profile (T2A), south profile (T2B), north profile (T2C).

Intermediate Dune GPR Profiles

The main GPR profile for the intermediate dune (27° 25’ 01.3” N, 97° 18’ 03.0” W) is the southernmost transect of the three study sites and is located approximately 150 m north of the beach access Park Road 22. The maximum height of the dune is 2.69 m. The profile starts at the backbeach from the highest wrack-line and extends 34.75 m over the back-side of the dune. The total width of the dune is approximately 22 m and has a well-developed berm that is accreting on the seaward side. There is a significant amount of vegetation cover starting on the berm, which increases in density on the landward side of the dune crest (see study area section for detailed description of vegetation types). Across the beach, there is a large accumulation of flotsam and jetsam that consists of both natural and human-made debris. Around these clumps of debris and especially within clusters of dense Sargassum seaweed, the foreshore is fronted with coppice dune fields where sand is trapped as it blows landward across the beach.

Along the GPR profile from a position of 0-10 m there are sub-horizontal shingled, gently seaward-dipping reflectors that persist through the section to a maximum depth of 4 m (Figure 16). An anomaly is present at the start of the profile that may be attributed to either interference or perhaps a metal object. The beach-dune interface is located at the 11 m position and is marked by a sharp “step” towards the dune. At the berm (12-15 m), on the seaward side of the foredune, there are discontinuous sub-horizontal steeply-dipping reflectors that transition into nearly horizontal reflectors continuing through the dune. On the landward side of the dune-crest there are sub-horizontal, landward-dipping reflectors that continue to the end of the

transect. The most notable feature that extends throughout the entire profile is the bright, nearly horizontal reflector. This strong reflector is bounded by small, low-amplitude, discontinuous convex undulating reflectors.

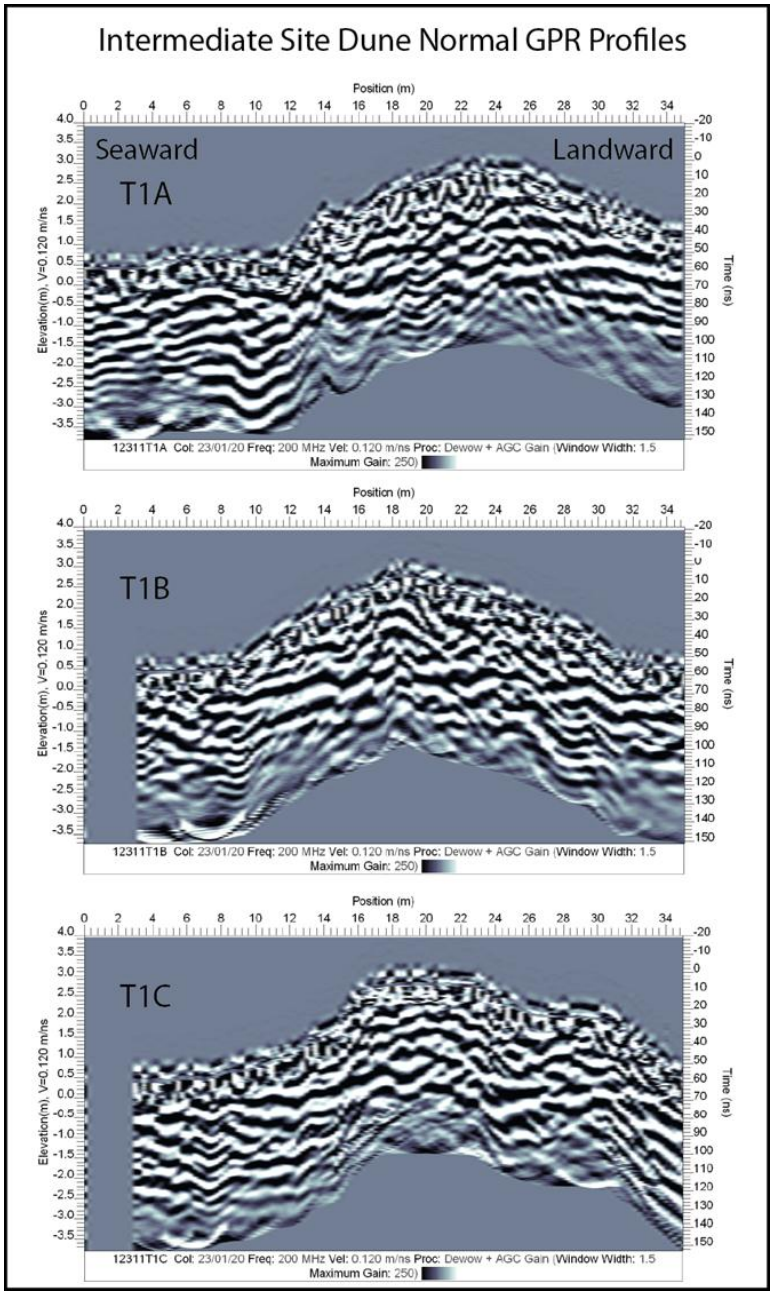

Figure 16. Intermediate dune normal GPR profiles; main profile (T1A), south profile (T1B), north profile (T1C).

Large Dune GPR Profiles

The main GPR profile at Site 3 (27 26’ 03.8” N, 97 17’ 36.4” W) is located approximately 100 m north from the northern end of the Malaquite Beach Campground. It is the northernmost site of the three study sites. This site represents the largest dune surveyed in this study with a maximum height of 3.77 m. Compared to the other two sites; this dune is also the narrowest with a width of approximately 11 m. The main profile starts at the backbeach, beyond the high-tide line and has a significant accumulation of wrack-line debris. Similarly to the intermediate dune, this site has a substantial amount of vegetation cover that begins on seaward side of the foredune and increases considerably on the backdune, beyond the dune crest. Additionally, this dune has a small berm at its base but is not as extensive as the berm at the intermediate dune.

From the start of the GPR profile to the beach-dune interface (0-8 m) there are primarily gentle, nearly horizontal seaward-dipping reflectors that extend from a depth of 1.5-5 m (Figure 17). These reflectors are capped by higher-angle seaward dipping reflectors between depths of 0.5-1.5 m. At the base of the dune, there are discontinuous, lower amplitude convex reflectors. The reflectors then transition into high-angle, seaward-dipping reflectors (9-12 m) from the base of the dune towards the dune crest. The reflectors become nearly horizontal at the crest of the dune (12-16 m) and begin to dip landwards on the backdune from 16-20 m. On the back-side of the dune, the reflectors transition from landward to seaward dipping at the 24 m mark. Towards the end of the profile, the reflectors gently dip seawards from 25-29.5 m. Throughout the entire profile there are several anomalies between 0-0.5 m, 3-4 m, 10.25 m, 16 m, 18.75

m, and 27.5-29.5 m. These anomalies can be a result of interference from debris such as metal objects, time zero offsets during data acquisition and/or guided waves.

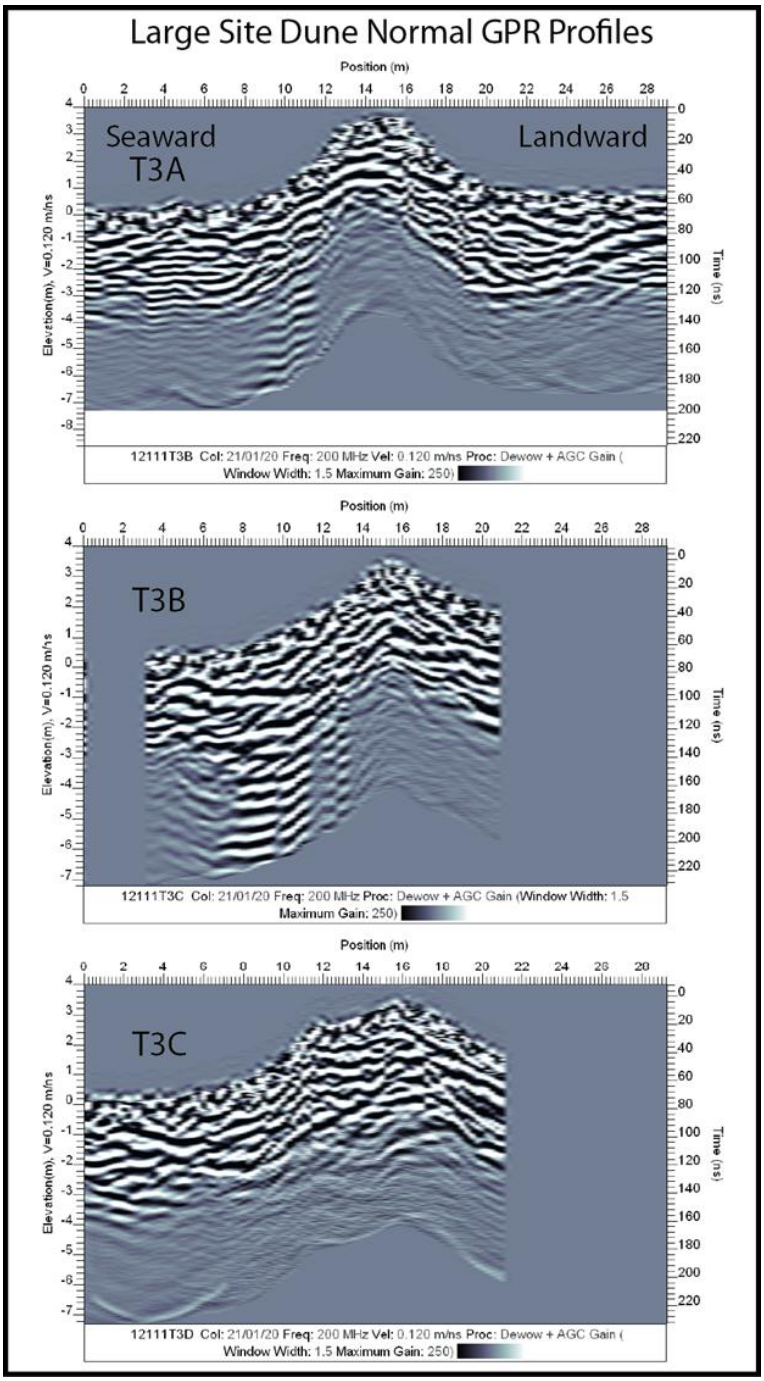

Figure 17. Large dune normal GPR profiles; main profile (T3A), south profile (T3B), north profile (T3C).

In addition to the dune normal profiles, one dune parallel transect was collected at each site (Figure 18). The alongshore GPR profiles for the small and intermediate dune show gently-dipping sub-horizontal reflectors. The reflectors within the small dune profile change dip from south to north at the 8 m position along the profile. There is a bright, horizontal reflector at a depth of approximately 120 cm, coinciding with the interpreted storm surface for the main small dune transect (T2A). The radar reflectors within the intermediate dune GPR profile gently dip to the north. A bright reflector occurs at the intersection with the main GPR transect (T1A) at the same depth of the interpreted storm surface. Both small and intermediate dune sites exhibit comparable, linear reflector geometries. However, the alongshore radar profile from the large dune site shows packages of trough-cut and fill and lacks the structure seen within the small and intermediate dune profiles. The hyperbolic responses occurring below 3 m within the large dune profile are most likely a result of over-migration during data processing. In other words, below the 3 m horizon, the radar wave velocity decreases with increasing moisture content.

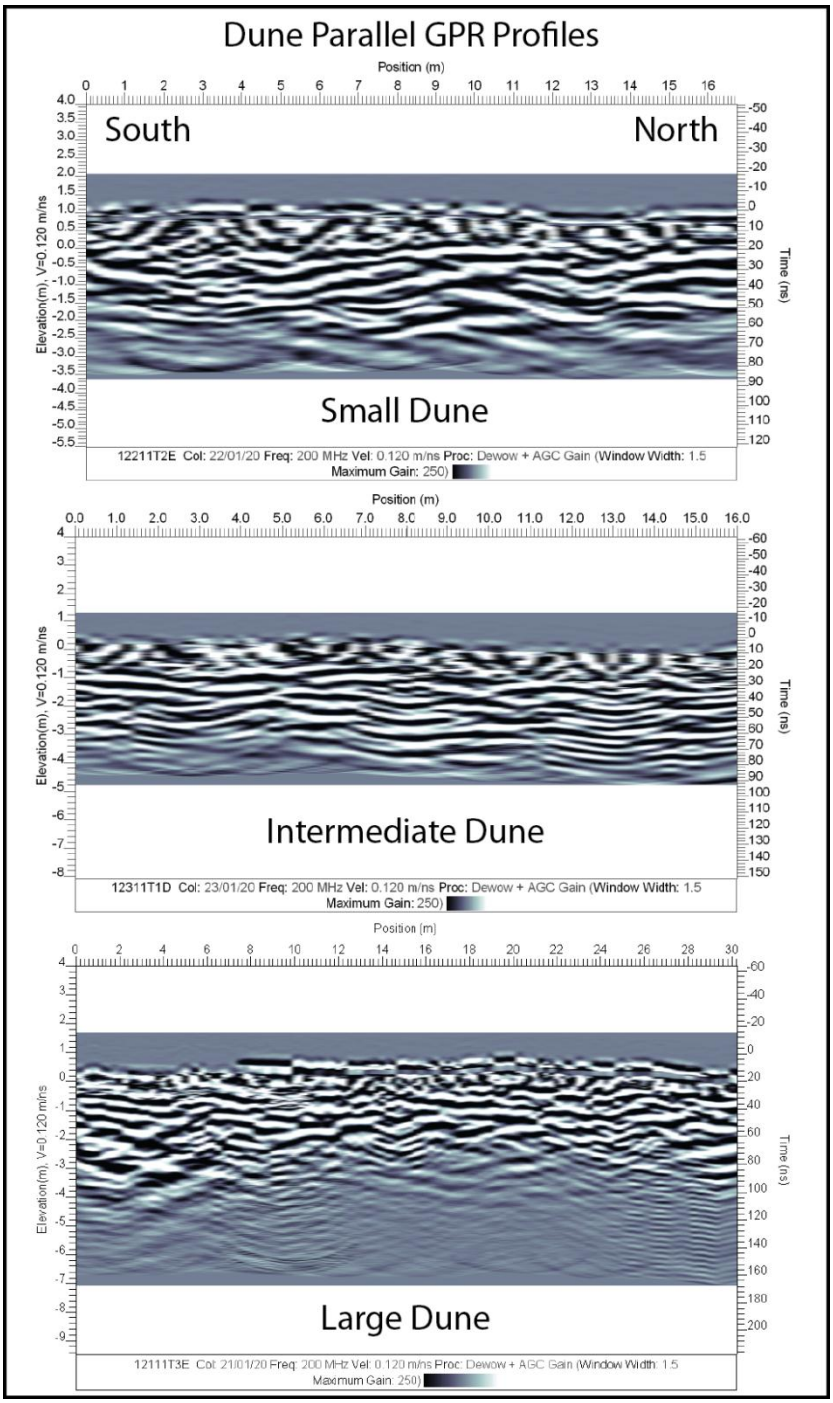

Figure 18. Dune parallel profiles for each site.

GPR Profile Comparisons

The GPR profiles show distinct structural differences between small, intermediate and large dunes, where the reflectors are interpreted to represent primary sedimentary structures. Uncomformities at reflector terminations define the location of related packages of strata and are separated by radar sequence boundaries (Bristow et al., 2000b). Reflector events with similar characteristics are interpreted to represent different radar facies. These radar facies, constrained by sequence boundaries, provide the basis for interpretation for the main profiles (i.e., T1A, T2A, T3A) at each site. It is important to note that with the 200 MHz antennae and the radar wave velocity of 0.12 m ns^{-1} obtained from CMP analysis, individual laminae or forests at a resolution below 12.5 cm cannot be resolved. However, packages of sedimentary structures greater than 12.5 cm at reflector terminations (i.e., radar sequence boundaries) can be determined. Bristow, et al. (2000) suggests that certain sequence boundaries can be linked to erosion events that are likely caused by storms. Bounding surfaces that extend horizontally from the beach to the dune are most likely erosional surfaces caused by storm surge and have been termed storm surfaces (Bristow et al., 2000b). These storm surfaces can be identified by a persistent, continuous horizontal reflector that extends laterally throughout the GPR transect. It is argued that several profiles along the small and intermediate dune sites exhibit a characteristic storm surface and provides the basis for a storm impact model discussed at the end of this section. In addition to storm surfaces, the radar profiles for each site commonly show packages of foreslope accretion, rearslope accretion, trough cut and fill, beach and swash bar deposits (Bristow and Bailey, 2001; Bristow et al.,

2000b). The subsequent explanations for each study site in the discussion follows standard radar facies interpretations used in coastal and eolian dune studies (Bristow and Bailey, 2001; Bristow et al., 2000a; Bristow et al., 2000b; Neal, 2004).

VIBRA-CORE RESULTS

Visual core descriptions, grain size statistics and XRF results are presented in the following sections to show relationships between normalized Ca spikes from XRF data to the four grain size parameters; mean grain size (ϕ), sorting (σ), skewness (Sk) and kurtosis (K) (note normalized kurtosis values obtained from equation 5). The following diagrams (Figures 21 and 28-38) provide descriptions of organic and shell layers and are indicated by dark triangles and open circles respectively. Normalized calcium (Ca) count XRF data is presented for each core obtained by the following equation:

$$N = \frac{peak\_area\_element}{\sum peak\_areas} \times 100 \qquad (8)$$

Increasing Ca counts down-core correspond to characteristic changes in grain size parameters that include poorly sorted, negatively skewed and increased (normalized) kurtosis values. Visible shell has layers are not always associated with Ca spikes, which can be attributed to a narrow sampling window of the X-ray beam. Applying a small X-ray spot with sample diameters ranging from 100 to 20 μ, means that only a few grains are analyzed per sample position. However, if the Ca signal within laminated sediments is clearly present, even relatively low counts from the XRF analysis is sufficient for analysis and interpretation.

Textural classifications from grain size analysis indicate all core samples are very well-sorted, fine-grained sand. Small concentrations of heavy minerals determined from sieving (ie > 75 μ) are present throughout the cores and typically concentrated in close

proximity to shell layers. The composition (i.e., mineralogy) was determined for the intermediate dune beach core by X-Ray Diffraction (XRD) analysis to investigate whether there are significant compositional changes downcore. Five samples were analyzed at 0, 60, 100, 110, and 120 cm respectively. Each sample showed five characteristic peaks that correspond to a dominant quartz (SiO_2) signature (Figure 19). The results from each XRD sample determined that the sand is nearly 100% quartz, with a few minor impurities occurring at 110 and 120 cm. Therefore, there is virtually no significant compositional change except at the shell layer in the intermediate dune beach core.

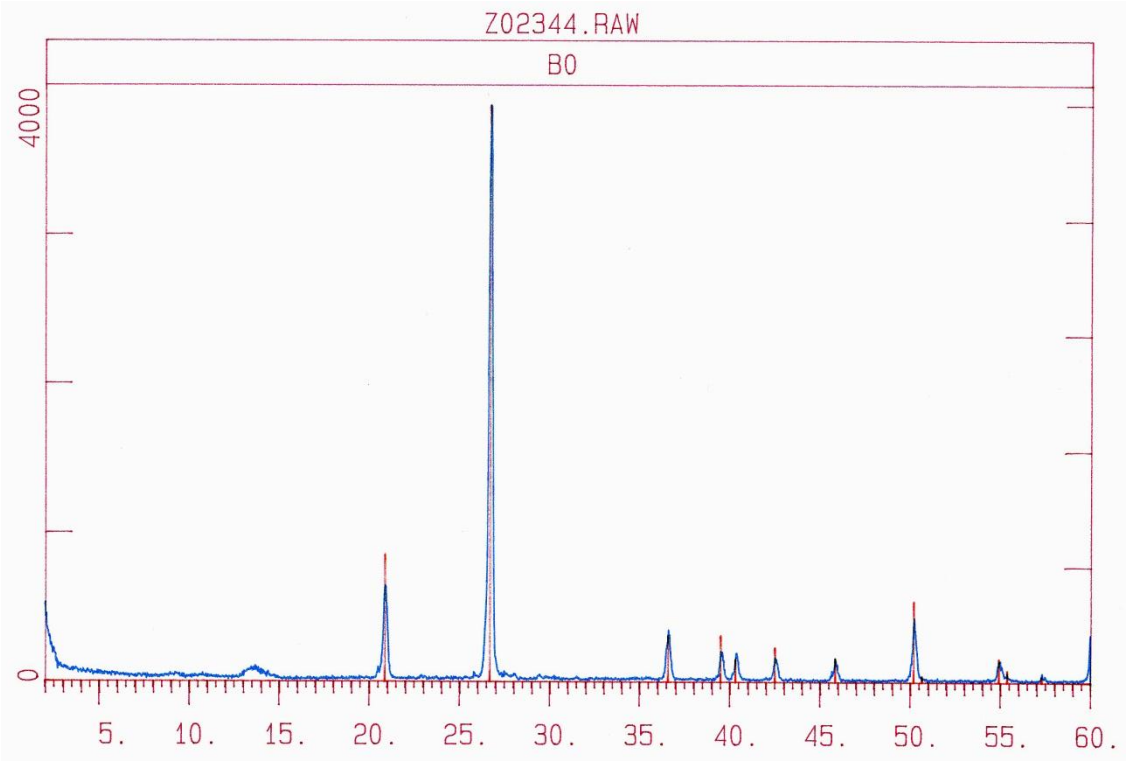

Figure 19. Example of XRD peaks for the intermediate dune beach core at 0 cm depth. The blue line represents the data with relative intensity (y-axis) versus beam angle (2θ). The peak identification card (33-1161) for quartz is superimposed to show the dominant quartz signature (pink line).

Small Dune Cores

Four cores were collected along the main GPR profile at the small dune site (27° 25’ 43.8” N, 97° 17’ 44.8” W) located at the southern end of the Malaquite Beach Campground (Figure 20). The maximum height of the small dune is 1.79 m and is approximately 15 m wide. Minimal vegetation covers the seaward side of the dune toe, but increases in density starting on the dune crest and extending landwards over the backdune. The small dune is flanked by larger dunes to the north and south (a few meters on either side) and is considered a transition zone between intermediate-sized dunes (greater than 2 m in height) that dominate this section of beach. The low-lying topography and marginal vegetation cover has allowed the dune to develop a small blowout. In contrast to the other two sites, this dune does not have a well-developed berm.

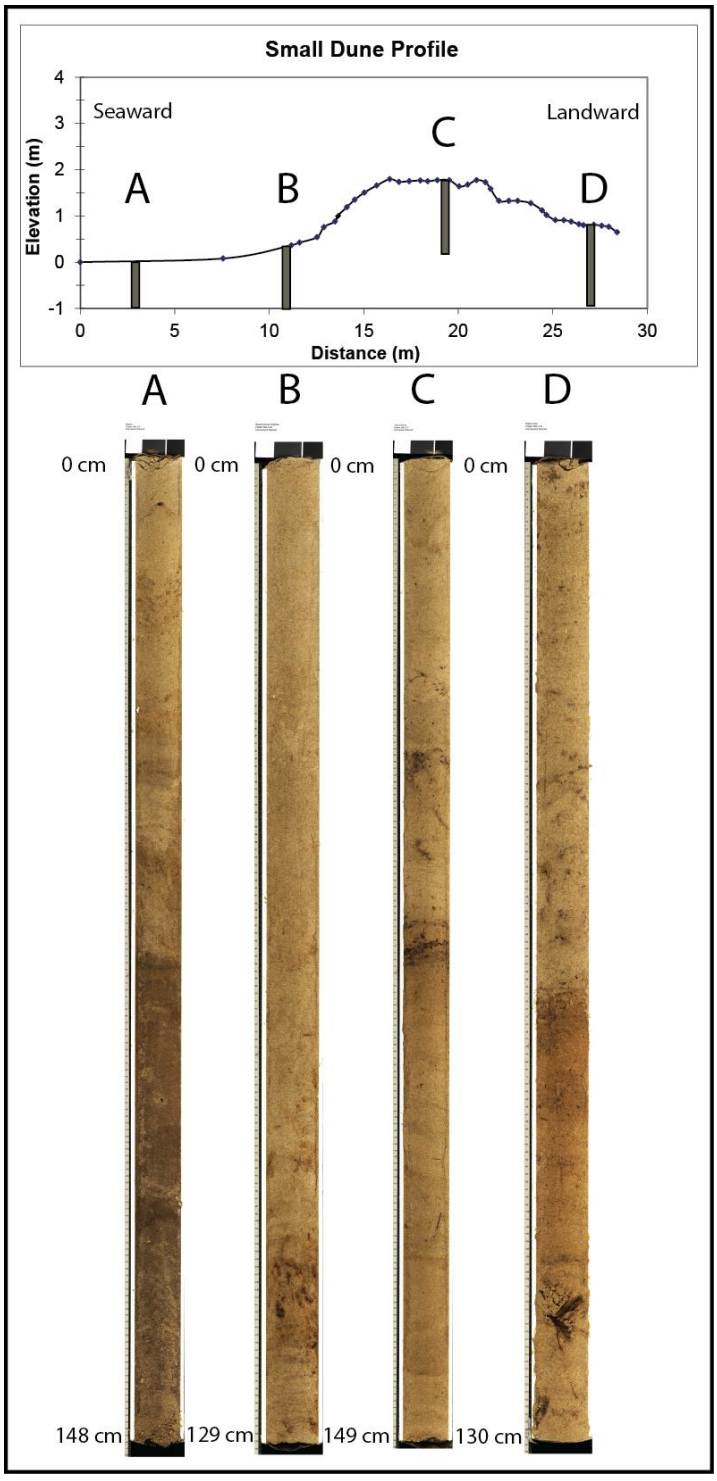

Figure 20. Small dune site vibra-cores and beach profile, showing relative locations. A) Beach, B) Beach-dune interface, C) Top of Dune and D) Backdune. The beach core (A) was taken at the start of the GPR profile along the backbeach

The first core (A) is located approximately 10 m seaward from the beach-dune interface, beyond the influence of the highest spring-tide, where the surface moisture decreases and is marked by wrack-line debris from past storm activity (Figure 21). There is a visible increase in moisture content at 74 cm that is marked by a dark color change within the core, which could represent a shallow water table. A large shell hash layer is clearly visible within the core and corresponds to a sharp increase in Ca counts between the 116-148 cm intervals. There is a direct correlation between Ca counts and grain size parameters, marked by a transition from fine to coarser mean grain size, poor sorting, negative skewness and increased kurtosis. Above the 120 cm interval there is little change in both grain size parameters and Ca counts.

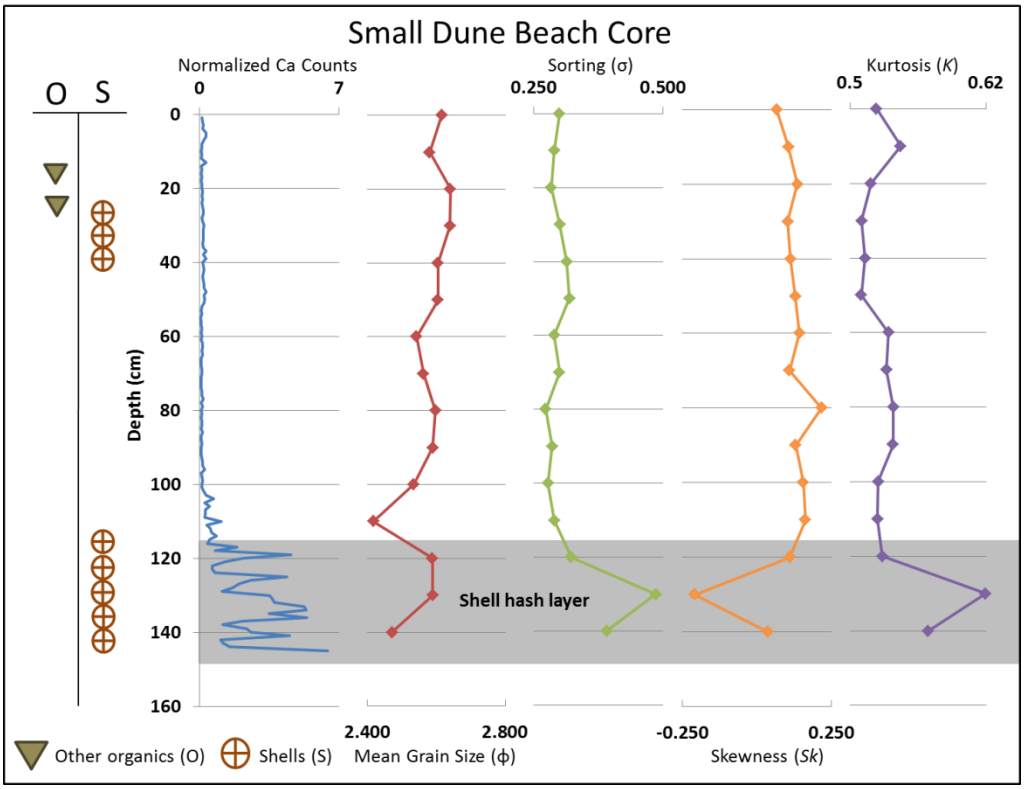

Figure 21. Small dune beach core plot showing visible organic layers, normalized Ca counts and grain size parameters.

The second core (B) is located 10 m landwards from the beach core at the base of the dune along the beach-dune interface (Figure 28 in the Appendix). Accumulations of seaweed are present along the backbeach from past storm surge although minimal vegetation is present along the base of the dune. Moisture increases within the core below 100 cm. Several organic layers are found between 90-130 centimeters and are terrestrial in origin. There are a few shell fragments present at 120 cm, but not enough to comprise a shell layer. The low Ca counts are highly variable and do not show a sharp increase that would indicate a shell horizon. Mean grain size increases slightly down-core with a peak at 120 cm. The sediment becomes poorly sorted and negatively skewed at 120 cm, although kurtosis on average remains fairly consistent. Please refer to the appendix for core locations and descriptions on all subsequent Figures.

The third core (C) was taken at the top of the dune, 5 m landward of the beach-dune interface (Figure 29 in the Appendix). An increase in vegetation cover occurs along the dune crest and increase significantly landwards towards the backdune. There is not a visible increase in moisture content within this core. Decayed sea oats (*Uniolapaniculata*) and other beach flora are found between 30-80 centimeters down-core. There are no visible shell fragments or shell hash layers present in this core, which is supported by the low concentration of Ca counts. Mean grain size fluctuates considerably, especially between the top of the core to a depth of 90 cm with a decreasing trend below 100 cm. The lower sorting values signify better sorting along the upper-half of the core. Skewness varies considerably throughout the core with positively-skewed intervals occurring at 20, 60 and 130 cm respectively indicating an

excess of fine grains (fine tails). Kurtosis displays an increasing trend down-core with a sharp decrease at 130 centimeters.

The fourth core (D) was taken at the end of the GPR profile, 15 m landward from the beach-dune interface (Figure 30 in the Appendix). Despite dense vegetation cover, it was possible to successfully extract a core in a clearing along the backdune. There is no significant increase in moisture content within this core. Similarly to the top of dune core, there are several organic layers beginning at the top of the core and increase in density down-core. For example, the backdune core contains a large stem of sea oat (*Uniolapaniculata*) between 111-118 centimeters. There is a large intact shell between 22-23 centimeters, however, no additional shell fragments or shell hash is present down-core. Ca counts fluctuate slightly but do not indicate any significant increase in concentration. An increasing trend in mean grain size is persistent from the top of the core to a depth of 50 cm, decreasing to 100 cm and then increasing to a peak at 120 cm. The core becomes progressively better sorted with depth, except at the 110 cm interval. There are two intervals with an excess of fines that are positively skewed at 40 cm and between 60-90 centimeters. Kurtosis values alternate with increasing trends between 10-40 and 110-130 cm and decreasing trends between 40-60 cm and 70-110 cm.

Intermediate Dune Cores

Three cores were collected along the main GPR profile at the intermediate dune site (Figure 31 in the Appendix). This site is the southernmost transect of the three study sites and is located approximately 150 m north of the beach access Park Road 22 (27°

25’ 01.3” N, 97° 18’ 03.0” W). The maximum height of the dune is 2.69 m. The profile starts at the backbeach from the highest wrack-line and extends 34.75 m over the back-side of the dune. The total width of the dune is approximately 22 m and has a well-developed berm that is accreting on the seaward side. There is a significant amount of vegetation cover starting on the berm, which increases in density on the landward side of the dune crest. Across the beach, there is a large accumulation of detritus that consists of both natural and human-made debris. Around these clumps of debris and especially within clusters of dense Sargassum seaweed, the foreshore is fronted with coppice dune fields where sand is trapped as it blows landwards across the beach (see Figure 2).

The beach core (A) is located at the beginning of the GPR profile, 10 m seawards from the beach-dune interface (Figure 32 in the Appendix). The core was taken in an area extending past the highest wrack-line storm deposits and beyond the influence of the highest spring-tides. There is an increase in visible moisture content at 62 cm marked by a dark color change. A visible shell hash layer occurs at a depth of 120 cm. There are two spikes in Ca counts that occur at approximately 110 and 120 centimeters. Mean grain size increases down-core with a slight decrease at 110 cm and reaching a maximum at 120 cm. The general trend in sorting increases with depth, reaching a maximum at the 110 cm interval (poorly sorted) and becomes better sorted at 120 cm. Below 20 cm, skewness remains relatively consistent, decreasing between 90 and 110 cm and increasing to a maximum at 120 cm. Kurtosis values sharply increase at 50 cm and decrease to 70 cm with a slight increase further down-core.

The second core (B) is located at the base of the dune along the beach-dune interface (Figure 33 in the Appendix). The base of the dune is fronted by a berm that is accreting seawards. At 100 cm, there is a significant increase in moisture content. Several organic horizons consisting of partially decayed beach vegetation lie between 24-32 and 74-80 cm. A piece of what appears to be charcoal is present at the 16-17 cm interval. Visible shell hash layers occur between 110 and 120 cm coinciding with the sharp Ca count spike in the XRF data. Mean grain size steadily increases below 30 cm with a maximum at 110 cm, consistent with the Ca count spike. Sorting remains comparatively stable down-core, becoming poorly sorted at 110 cm. The sample from 110 cm is negatively skewed, although kurtosis is stable across the shell hash layer.

The third core (C) is located on top of the dune, approximately 15 m landwards from the beach-dune interface (Figure 34 in the Appendix). Although the top of the dune is densely covered with vegetation, there are remarkably few organic horizons within the core. Unlike the beach and beach-dune interface cores, there is not a visible increase in moisture content within this core. Organic material is present at the surface (0-8 cm), between 97-99 and 120-125 cm. There are no visible shell fragments or shell layers in this core. A small spike in Ca counts occurs at 5 cm; however, the counts fluctuate around 1% throughout the rest of the core. Mean grain size increases linearly until 50 cm, followed by sharp decreases and increases in size throughout the remainder of the core. Sorting nearly follows the exact opposite trend as mean grain size and is poorly sorted at 70 and 130 cm respectively. The samples become progressively well sorted between 70 and 110 cm. Two positively skewed peaks coincide with the 60 and 110 cm

intervals. Kurtosis values generally follow an increasing trend and reach a maximum at 40 cm and a minimum at 110 cm.

Large Dune Cores

Four cores were collected along the main GPR profile (Figure 35 in the Appendix). The site is located approximately 100 m north from the northern end of the Malaquite Beach Campground (27 26' 03.8" N, 97 17' 36.4" W). It is the northernmost site of the three study sites. This site represents the largest dune surveyed in this study with a maximum height of 3.77 m. Compared to the other two sites; this dune is also the narrowest with a width of approximately 11 m. The main profile starts at the backbeach, beyond the high-tide line and has a significant accumulation of wrack-line debris. Similarly to the intermediate dune, this site has a substantial amount of vegetation cover that begins on seaward side of the foredune and increases considerably on the backdune, beyond the dune crest. Additionally, this dune has a small berm at its base, but is not as extensive as the berm at the intermediate dune. Although four cores were taken at this site, erroneous XRF results from the beach core are not presented. There is a large intact shell at the 117-121 cm interval that was removed to prevent damage to the protective film covering the helium-flushed X-ray optical system. Ca counts from the duplicate beach core are plotted, ceteris paribus, with the grain size results from the original beach core (Figure 36 in the Appendix).

The beach core (A) is located at the beginning of the GPR profile, 8 m seawards from the beach-dune interface (Figure 36 in the Appendix). The second core (B) is a duplicate beach core taken adjacent to the primary beach core, offset by approximately 1 m. Visual core descriptions and grain size results are presented from the original beach core, with Ca count XRF data taken from the beach-duplicate core. There are visible increases in moisture content at 84 cm and 65 cm for the beach and duplicate beach cores respectively. The beach core has a stained organic layer at 53-63 cm, with evidence of bioturbation. Shell fragments occur at 74-77 cm with a large intact shell and shell hash layer between 117-129 cm. Ca counts from the duplicate beach core are vertically offset by approximately 10 cm, but do coincide with the visible shell layer from the original beach core. The Ca counts have the highest concentration of all the cores from the three sites. It is reasonable to expect Ca counts of similar magnitude for the original beach core at the 117-121 cm interval. Mean grain size fines at the 20 and 50 cm intervals and coarsens at 40 and 120 centimeters. Sorting follows a similar and opposite trend to grain size with the poorest sorting at 10 cm, becoming well sorted at 40 cm with little change further downcore. Skewness values decrease from 10 to 30 cm with a sharp increase at 40 cm and continue to trend towards more negative values towards the bottom of the core. Kurtosis values decrease slightly from 10 to 30 cm, follow an increasing trend until 70 cm and marginally fluctuate further down-core.

The third core (C) is located along the beach-dune interface, approximately 10 landwards from the beach core (Figure 37 in the Appendix). There is a seaward accreting berm along the base of the dune, which is stabilized by vegetation cover. Unlike the beach cores, there is not a visible increase in moisture content within this core. Several visible organic horizons persist from 10 to 110 cm down-core. A large shell fragment is present at 47-49 cm, but there is not a shell layer present in this core. The Ca counts fluctuate between 0.4 and 1.2 % and do not indicate any sharp increases. Mean grain size fines from 0-40 and 50-80 cm and increases from 40-60 and 110-140 cm. The coarsest grains occur at the bottom of the core at 140 cm. Samples become poorly sorted from 0-70 cm, become well-sorted at 80 cm and remain stable throughout the rest of the core. Skewness values generally decrease in trend from 0-70 cm, abruptly become positively skewed at 80 cm and decrease below 80 cm to a depth of 130 cm. There is a sharp decrease in kurtosis at the top of the core with an increasing trend from 10-60 cm. Kurtosis values decrease from 60-80 cm and remain fairly stable towards the bottom of the core.

The fourth core (D) is located on the backside of the dune, approximately 10 m landwards from the beach-dune interface (Figure 38 in the Appendix). There is no visible increase in moisture content within this core. A high degree of visible organic material is present throughout the core, including seeds at 136-139 cm. There are two visible shell horizons at 103-105 cm and 131-133 cm intervals containing large, intact shell tests. The corresponding Ca counts spike at these same intervals, indicating two small shell hash layers.

Mean grain size increases from 10-30 cm and decreases from 30-60 and 100-140 cm respectively. There is a sharp increase in grain size at 70 cm. The sample at 100 cm becomes well-sorted at the top of the shell hash layer and becomes more poorly sorted at 110 cm to the bottom of the core. At the 100 cm interval, there is a sharp decrease in skewness and decrease in kurtosis signifying a coarse tail in the distribution.

Comparison of Storm Surfaces between Sites

Close-up images of the beach cores for the three sites are presented in Figure 22 comparing the storm surface locations at each site. There is a slight vertical offset of the storm layers where the storm surface is identified at 118 cm, 120 cm and 118 cm for the small, intermediate and large cores respectively. The shell hash layers are relatively thin at the intermediate and large dune sites. Conversely, the shell layer at the small dune site extends from 118 cm to the bottom of the core at 147 cm and is the thickest shell layer between all three sites.

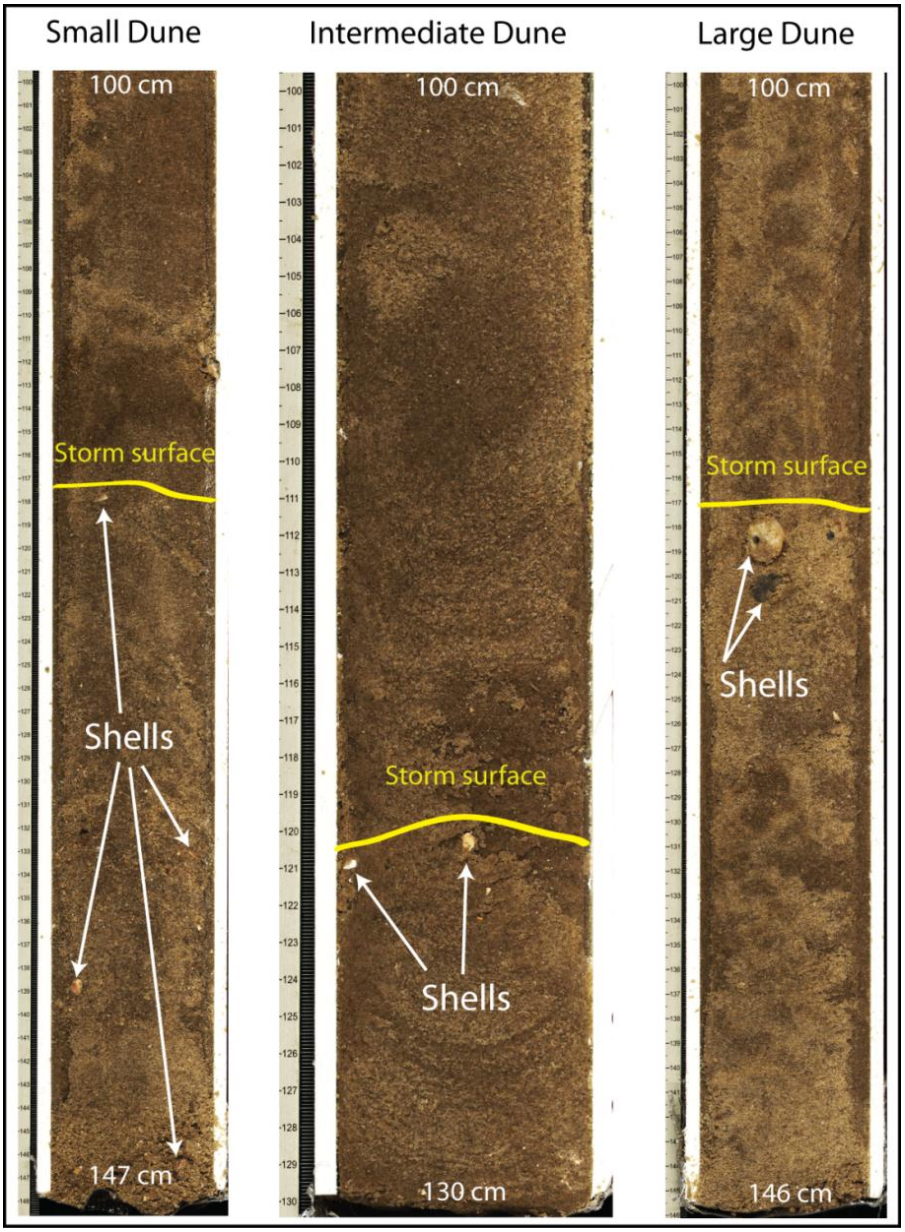

Figure 22. Comparison of storm surfaces between the small, intermediate and large dune sites (note the thick shell layer between 118-147 cm at the small dune site).

XRF Calcium Count Comparisons

Figure 23 compares relative calcium counts across the beach, beach-dune interface and dunes for each site. Additionally, Ca counts for the different environments

are compared between each site to show the relative concentrations in Figure 24. For the small dune, the strongest Ca count signature corresponds to the large shell hash layer at the bottom 30 centimeters of beach core. Ca counts for the other three cores across the small dune site are negligible compared to the beach core. There are three notable Ca count signatures along the intermediate dune transect. Two spikes occur at 110 and 120 cm for the beach core, but are relatively small in comparison with the beach-dune interface signature at 115 cm. The most significant Ca count spikes for the large dune transect occur within the duplicate beach core at 130 and 135 cm. However, it is reasonable to expect a large Ca spike at 120 cm within the original beach core that coincides with a large intact shell that had to be removed to prevent damage to the X-ray optical system. Two smaller peaks are present at 105 and 130 cm are located within the backdune core, but are small in comparison to the Ca counts from the duplicate beach core.

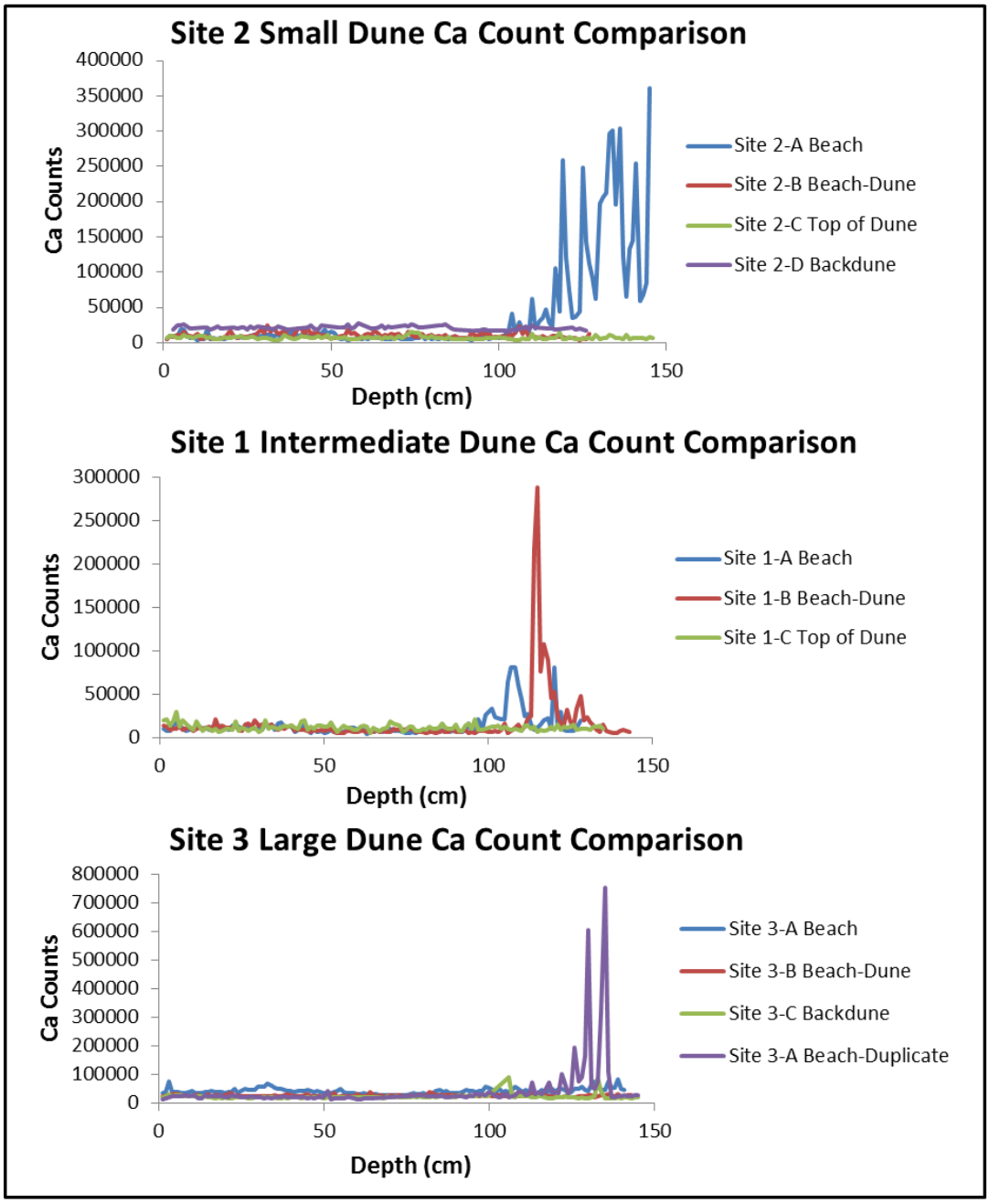

Figure 23. Comparison of Ca counts across the beach, beach-dune interface and dunes for each site.

Comparisons of each environment between sites are presented in Figure 24. Although the largest shell hash layer for all the cores occurs within the small dune beach core, the highest Ca counts for all the beach cores corresponds to the duplicate beach core at the large dune site. The Ca counts for the large dune duplicate beach core are more than twice that of the small dune shell hash layer. Comparing the Ca counts between the beach-dune interface cores reveals that the highest counts correspond to the intermediate dune site. The Ca counts for the intermediate beach-dune interface core are nearly six times greater than the other beach-dune interface cores. The Ca counts for the top of dune and backdune cores are the smallest of the three environments across the study sites. The two Ca spikes that occur within the large dune backdune core are relatively small in comparison with the beach and beach-dune interface cores. Nevertheless, the Ca spikes for the large dune backdune core are more than four times greater compared to the other dune cores.

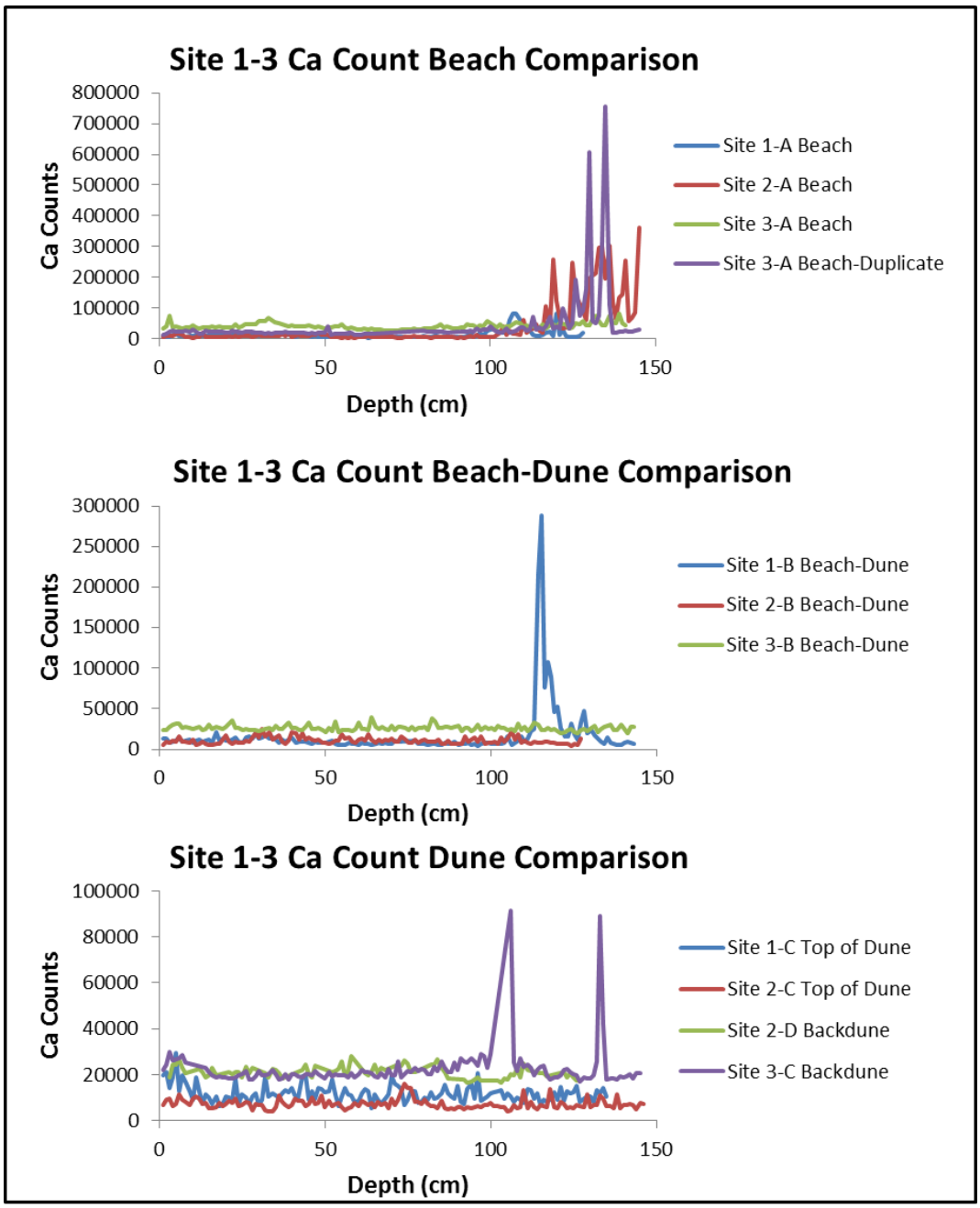

Figure 24.Comparison of Ca counts for each environment between the three study sites.

DISCUSSION

This study demonstrates the utility of GPR and vibra-coring to interpret depositional history and identify storm surfaces within the beach-dune system along the northern segment of Padre Island National Seashore, Texas. Through a combination of visual core descriptions; XRF scanning, grain size analysis and GPR profiles, the results suggest that the small, intermediate and large dune responded and recovered from the same storm event in different ways.

Interpretation of the Small Dune GPR Profile

The small dune is located in a transition area where the width of the backbeach and the location of offshore bars are between the intermediate and large dune sites. From the main GPR transect, several radar facies can be identified. The continuous, horizontal reflector that mirrors the surface topography at a depth of 1 m is interpreted as a storm surface and represents the first sequence boundary (Figure 25). From the beginning of the profile to 12 m, there is a package of low-angle, seaward-dipping reflectors that are characteristic of beach facies. Just above the beach deposits, there is a narrow section of short, seaward-dipping clinoforms that is interpreted to be a small swash-bar deposit. Extending along the profile from 12-22 m at a depth of 1-3 m is a package of convex reflectors that are interpreted as the dune core. Another sequence boundary is distinguished by a package of sub-horizontal, landward-dipping reflectors that are interpreted to represent rearslope accretion on the landward of the dune.

The lack of a well-developed berm suggests that unlike the intermediate-sized dune, this dune did not grow by the seaward advancement of embryo dunes. This dune exhibits similar characteristics to Level 3 "overwash regime" described by Sallenger (2000), where the storm surge overtopped the dune with little to no scour. As a result, the low-relief of the dune resisted significant change during storm inundation. As noted before, this dune also has less vegetation cover than the other two dunes which may also explain why the dune hasn't recovered in a similar way as the intermediate and large dunes. Swash-bar deposits suggests that this low-lying area may have been submerged for an extended period of time.

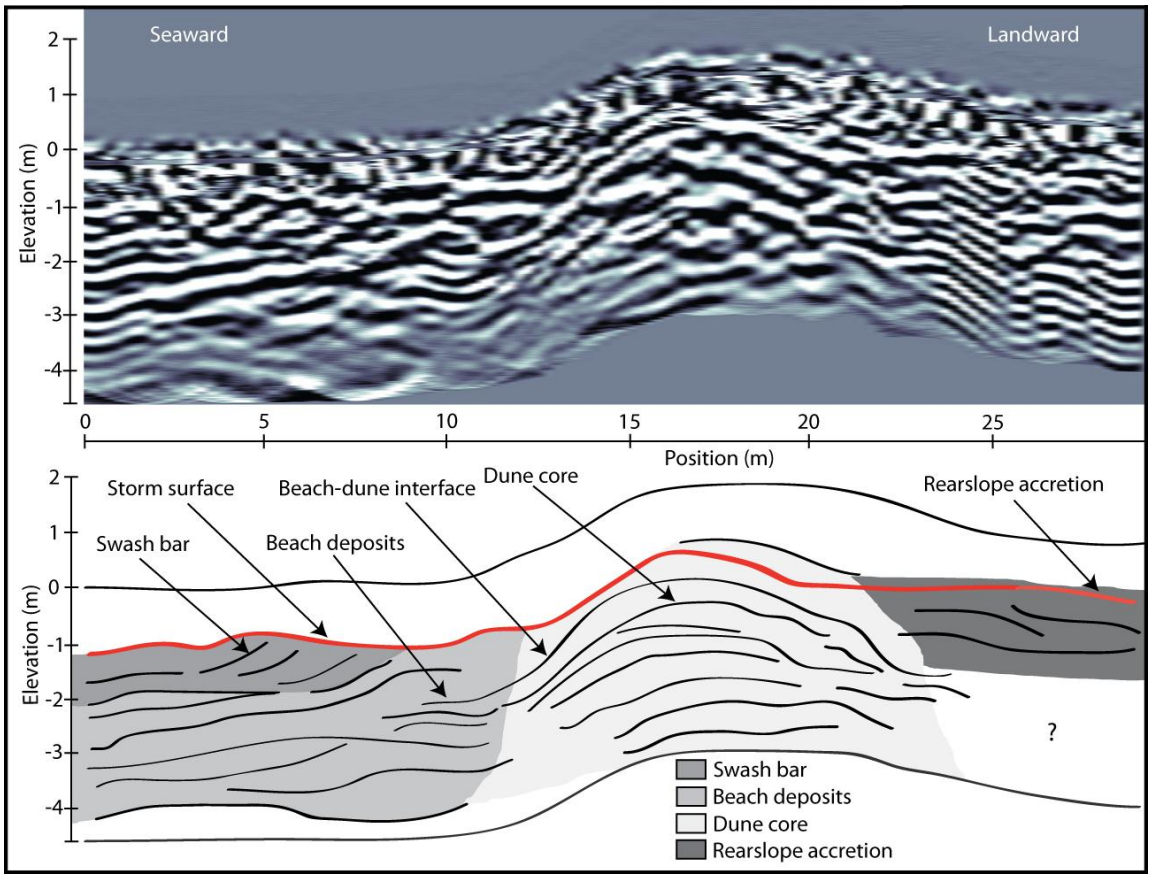

Figure 25.Small dune GPR profile and interpretation.

Interpretation of Intermediate Dune GPR Profile

The intermediate dune is located in an area where the offshore bars are furthest away and the beach width is greatest, compared to the other two sites. The most significant feature of the main GPR profile is the prominent sub-horizontal reflector that extends through the entire section at a depth of approximately 1 m (Figure 26). This reflector is interpreted as a storm surface and is identified as a radar sequence boundary. The convex reflectors directly above the erosional surface resemble small embryo dunes that may have developed as the beach-dune system recovered after the storm. The package of convex reflectors (14-26 m) begins at the modern beach-dune interface, where the most recent embryo dune has welded to the foredune. It is argued that as the embryo dunes accrete seaward, they provide a platform for the dune to grow vertically as eolian driven sediment became trapped by vegetation. Below this radar sequence boundary, there are a series of stacked, low angle (< 10°) seaward-dipping reflectors that are interpreted to represent beach deposits and represent another radar sequence boundary. They are laterally continuous for 12 m from the start of the transect. Approaching the beach-dune interface, the reflectors "step" and mimic the surface topography of the berm. It is assumed that the location of the berm must have changed over time and that the step feature is likely a processing artifact from shifting the topography. On the landward side of the dune crest, there is a package of landward-dipping reflectors that suggestrearslope accretion.

Based on existing theories and models of beach-dune interaction, it is argued that for a transgressive system it would be expected that the dune would migrate landward in

response to a relative rise in sea-level. However, it appears that this foredune is accreting towards the coast as the berm migrates seaward and widens the foredune platform which enables the dune to grow vertically over time.

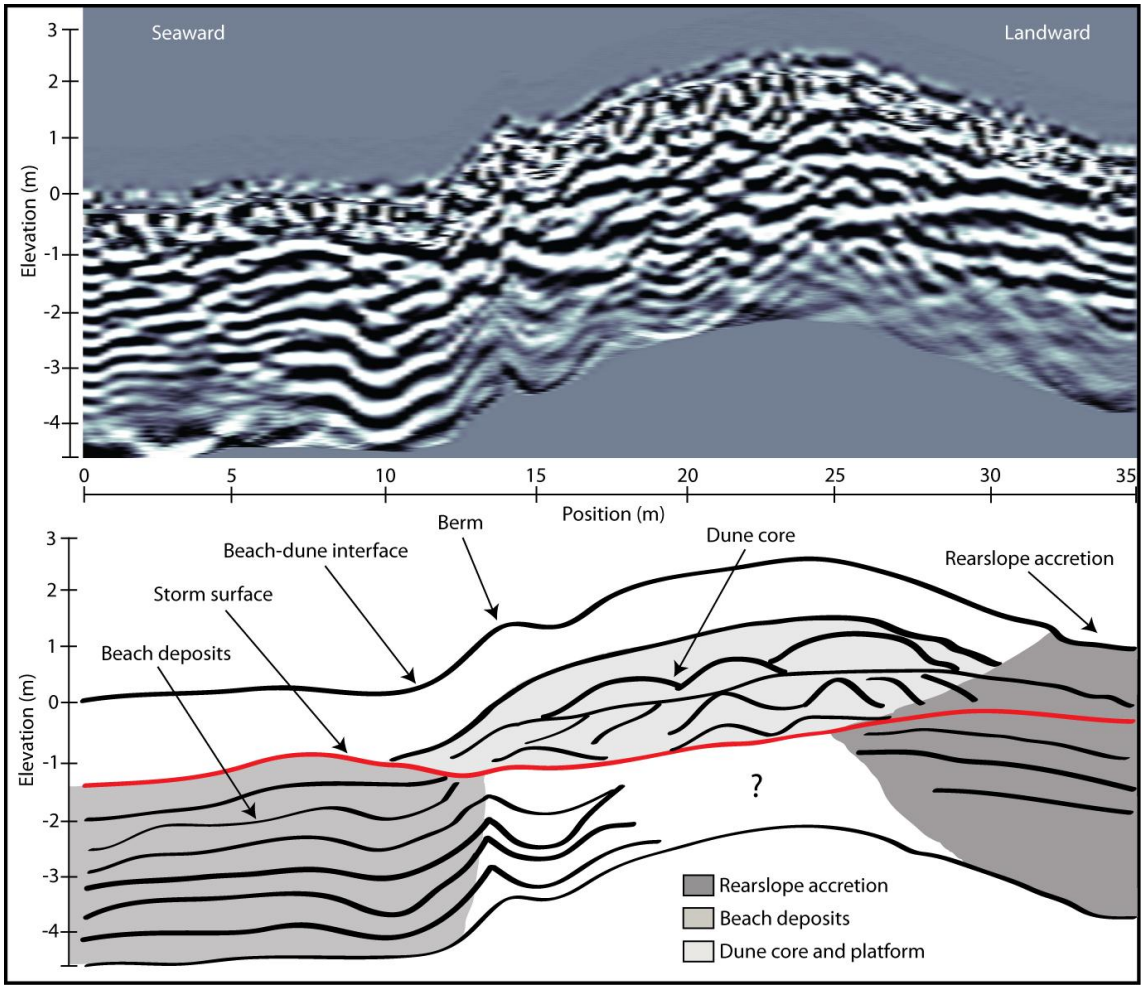

Figure 26.Intermediate dune GPR profile and interpretation.

Interpretation of the Large Dune GPR Profile

The large dune is located where the offshore bars are closest to the beach and the width of the beach is the narrowest for the three sites. The large dune has six interpreted

packages of strata that reveal the most complexity of all three sites (Figure 27). Similarly to the other sites there is a continuous horizontal reflector at a depth of 1 m and corresponds to the same storm surface seen at the small and intermediate dune sites. However, this storm surface is not continuous throughout the entire section, suggesting that the large dune was not completely inundated by the storm surge. Fronting the beach-dune interface (0-7 m) is a set of short, landward-dipping clinoforms that are indicative of represent swash bar deposits. Below this radar sequence boundary (2-4 m depth), there are a series of gently seaward-dipping reflectors that are indicative of beach deposits. At the 10 m position along the profile there is a deeply penetrating package of strong reflectors that coincide with the modern beach-dune interface. The fact that these deep reflectors are seen at the same depth and location along the south profile (T3B) suggests that these reflection events are real and not an artifact of processing or anomalies. These strong reflectors may represent an erosional channel and/or scour at base of the beach-dune interface.

The stacked, horizontal reflectors that cap the dune core provide further evidence that this dune has remained stable for a significant amount of time during and after storm activity. The discontinuous, low-angle landward-dipping reflectors show rearslope accretion from eolian sediments that were deposited on the landward side of the dune crest. Interestingly, the package of rearslope accretion is not continuous like the other two sites and actually transitions into a package of discontinuous, sub-horizontal shingled seaward-dipping clinoforms, which define another sequence boundary. These

reflectors are similar in character to the modern dune core and are interpreted as an older dune core which may have eroded during a previous storm.

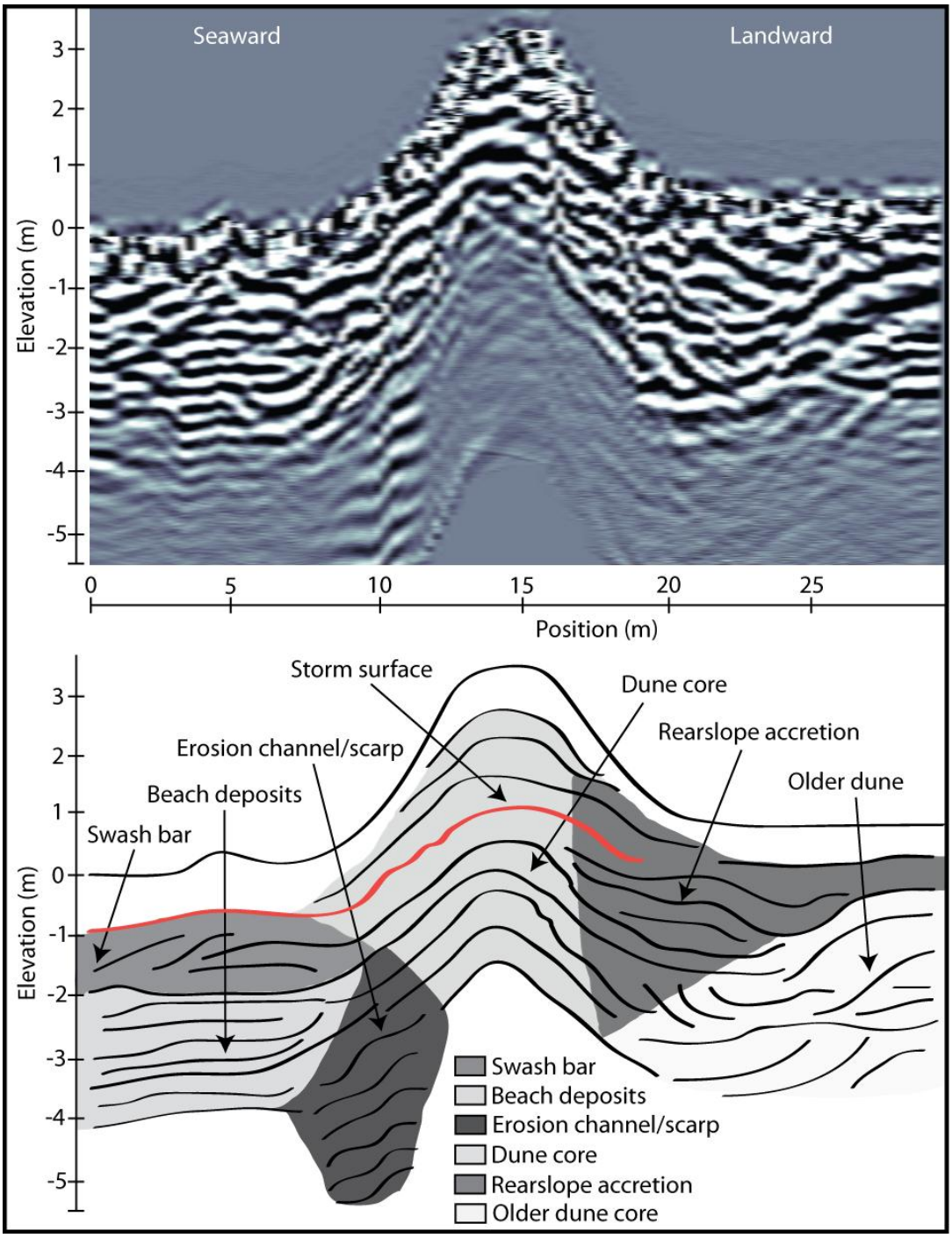

Figure 27.Large dune GPR profile and interpretation.

Storm Impact Model for Padre Island National Seashore

The study area between the South Beach access road Park 22 and the Malaquite Campsite exhibits considerable alongshore variation in beach-dune morphology. It is argued that the alongshore variability in dune height is influenced by the location of offshore bars and the geometry of the backbeach, both of which can regulate sediment availability and control dune growth over time. During a storm, the beach-dune system will respond and recover in different ways depending on the height and extent of theforedunes. Sallenger suggested that there will be variability in dune height along the same barrier island and explains that accurate and densely spaced topographic data is needed to better categorize storm impacts. Building upon the Sallenger (2000) storm impact model, this study utilizes GPR and vibra-cores to reconstruct past storm activity recorded in various-sized dunes along a relatively small stretch of beach (2.5 km).

The results from visual core descriptions, grain size analysis and XRF data suggest that shell hash layers occur with the backbeach cores at nearly the same depth (i.e., 120 cm) across the small, intermediate and large dune sites. It is argued that the location of each shell layer corresponds to a storm surface that was generated during a single storm. Assuming that the same storm event is recorded at each site, it is possible to interpret the morphological evolution and storm impact for the various-sized dunes. The response and recovery of the beach-dune system varies considerably alongshore within the 2.5 km study area. The presence or absence of the storm surface across the beach and dunes provides evidence for the height and extent of the surge during the storm event. The following discussion argues that: 1) there is a direct relationship

between grain size and Ca spikes in the XRF data, 2) the four grain size parameters can help distinguish transitions between beach versus dune signatures within the cores, 3) Identification of the storm surface from GPR, XRF and grain size analysis determines which regime impacted the beach-dune system at each site.

Visually identified shell layers and bright GPR reflectors coincide with sharp spikes in Ca counts from XRF scans, particularly within the beach cores at nearly the same depth across the three sites. The spikes in Ca counts correspond to an increase (coarsening) in mean grain size along the same interval within the cores. Samples become poorly sorted, negatively skewed and kurtosis values increase within the shell layers. Shell hash layers identified within the cores show a direct correspondence between Ca counts and mean grain size.

Grain size parameters can also be used to differentiate transitions from beach (marine) versus dune (eolian) environments (Mason, 1958). Because the sand along Padre Island is fine-grained and very well sorted, changes in mean grain size and sorting can only be slightly modified between beach and dune environments. Mason and Folk (1958) proposed that for beaches supplied by sediments uniform in grain size with exceptional sorting, subtle differences in transport modes (i.e., waves versus wind) affect the distribution of the tails considerably. Therefore, skewness and kurtosis provide the best measures to distinguish beach and dune environments. Assuming that the direction of sediment transport is predominately from the beach to the dunes (i.e., from higher to lower energy), mean grain size should decrease and become progressively well-sorted across the dunes. The addition of “fines” to the tails of the distribution means that an

eolian signature should be positively skewed with high kurtosis values. Conversely, the beach signature should be more negatively skewed with lower kurtosis values, poorly sorted with a larger mean grain size. By comparing the four grain size parameters for each core within the study sites general trends are described in the results section to distinguish beach versus dune environments.

Comparing changes in grain size parameters to the location of shell hash layers from visual descriptions and XRF scans facilitated the identification of each storm surface for the small, intermediate and large dune sites. Sallenger (2000) proposed that the determination of each impact regime depends on the ratios between dune height and the runup elevation during a storm event. The four regimes include; "swash regime," "collision regime," "overwash regime," and "inundation regime." The "swash regime" is defined to occur during a storm where the swash is restricted to the foreshore resulting in a net offshore transport of sediment, later returning to the beach during recovery. The "collision regime" occurs when the runup collides with the base of the dune, eroding the dune where the eroded sediment is transported offshore and/or longshore and is typically not returned to re-establish the foredune. As the runup height increases, the dune will be overtopped defining the "overwash regime," where sediment eroded from the dune is transported landward and not easily returned seaward. When the runup is large enough to completely submerge the foredune system the "inundation regime" occurs having detrimental impacts for the entire barrier island.

With high energy conditions during an extreme storm, the surge has the capability to erode fine-grained sediments and deposit larger-grained sediments from the

swash zone to create an erosional surface that can be overlain by significant accumulations of shell hash. Consequently, the vertical and landward migration of large-grained sediments leaves a "footprint" of the height and extent of the surge. Based on the location of each interpreted storm surface across the three study sites, the impact regimes are classified in the following way.

Grain size analysis and XRF results from the small dune site show the largest storm surface at 120 cm depth within the beach core. Despite the absence of a Ca count spike at along the beach-dune interface, an increase in mean grain size, poor sorting and negative skewness suggests that there is a beach environment signature at 120 cm. The GPR results further suggest that for the small dune, the interpreted storm surface (at a depth of 120 cm) extends laterally throughout the radar profile to the backdune. The presence of an erosional layer beyond the dune crest implies that the dune was completely submerged by the surge. Thus, the storm impact for the small dune is interpreted to represent a transition from "overwash" to "inundation regime".

The intermediate dune has an interpreted storm signature within the beach and beach-dune interface cores at a depth of 120 cm. The radar profile from the GPR study shows a bright, laterally continuous reflector at approximately the same depth that extends horizontally through the dune. Interpretation of the GPR profile suggests that the dune was completely eroded during the storm event. Subsequently, the erosional surface provided a platform for the dune to grow vertically through the seaward extension of embryo dunes. Therefore, the intermediate dune represents a transition from "collision" to "overwash" regimes.

Beach and duplicate beach cores from the large dune also contain a storm surface at 120 cm down-core. A storm signal is not present within the beach-dune interface core and there are no laterally continuous radar reflectors in the GPR profile for this site. The interpreted cut-trough and fill radar facies suggest that during the storm, scour occurred along the base of the dune but the surge did not overtop the dune crest. Thus, the large dune corresponds to "collision regime."

Evidence from visual core descriptions, XRF data, grain size analysis and GPR profiles indicates a storm layer persists at a depth of 120 cm along the backbeach at each of the three sites, with some landward extension at the small and intermediate dune sites. It is argued that the dunes responded to the surge from the same storm in very different ways. The small dune was overtopped by the surge, experienced little net erosion and minimal recovery. The intermediate dune was completely eroded by the surge, but showed the greatest recovery of all the dune sites. The large dune was scoured at the base with marginal impact along its crest and shows minimal recovery after the storm.

CONCLUSION

This study demonstrates through the use of GPR that there are structural differences between large, intermediate and small dunes along North Padre Island. These findings suggest that even along a relatively small stretch of beach, subtle variations in dune height and extent will affect how the dunes change over time. Results from the interpreted GPR profiles and vibra-cores show evidence of past storm activity, suggesting that alongshore variability in dune height governs how the beach-dune system responds and recovers from extreme storms. It is argued that the location of offshore bars and backbeach geometry play a significant role in controlling the amount of available sediment to the foredunes.

The large dune is found where the offshore bar is closest to the beach and backbeach is the narrowest. The intermediate dune is located in an area where the offshore bars are furthest away and the backbeach is the widest. The small dune is situated between these two end members. The most significant features from GPR surveys across the three sites are the strong, laterally continuous reflectors that are interpreted as storm surfaces (i.e., erosional surfaces). Different characteristic radar facies and sequence boundaries surrounding the storm surface provide evidence as to how each dune evolved after the storm.

Impact scales for the small, intermediate and large dune based on radar facies and sequence boundaries for each profile correspond to inundation, overwash and collision regimes respectively. The small dune representing a transition from “overwash”

to “inundation regime” was overtopped by the surge, experienced little net erosion with minimal recovery. The intermediate dune signifying a transition from “collision” to “overwash regime” was completely eroded by the surge, but showed the greatest recovery of all the dune sites. The large dune demonstrating “collision regime” was scoured at the base with marginal impact along its crest and shows minimal recovery after the storm. These findings suggest that within the 2.5 km study area, there is considerable variation in how the three different-sized dunes responded to and recovered from storm activity. It is proposed that further research is needed to refine storm impacts at higher-resolution within small stretches of the same beach.

REFERENCES

Aagaard, T., Davidson-Arnott, R., Greenwood, B., and Nielsen, J., 2004. Sediment supply from shoreface to dunes: linking sediment transport measurements and long-term morphological evolution. Geomorphology 60, 205-224.

Abuodha, J.O.Z., 2003. Grain size distribution and composition of modern dune and beach sediments, Malindi Bay coast, Kenya. Journal of African Earth Sciences 36, 41-54.

Alagarsamy, R., Zhang, J., 2010. Geochemical characterisation of major and trace elements in the coastal sediments of India. Environmental Monitoring and Assessment 161, 161-176.

Bailey, S., Bristow, C., 2000. The structure of coastal dunes: Observations from ground penetrating radar (GPR) surveys. Proceedings of the Eighth International Conference on Ground Penetrating Radar 2000, University of Queensland, Australia, pp. 660-665.

Blott, S.J., Pye, K., 2001. GRADISTAT: A grain size distribution and statistics package for the analysis of unconsolidated sediments: earth surface processes and landforms 26, 1237-1248.

Boggs, S.J., 2001. Principles of Sedimentology and Stratigraphy, 3rd edition. Prentice Hall, New Jersey.

Bristow, C., 1995, Facies analysis in the Lower Greensand using ground-penetrating radar. Journal of the Geological Society 152, 591-598.

Bristow, C., Pugh, J., Goodall, T., 1996. Internal structure of aeolian dunes in Abu Dhabi determined using ground-penetrating radar. Sedimentology 43, 995-1003.

Bristow, C.S., Bailey, S.D., 2001. Non-invasive investigation of water table and structures in coastal dunes using ground-penetrating radar (GPR): implications for dune management. Coastal Dune Management - Shared Experience of European Conservation Practice, pp. 408-417.

Bristow, C.S., Bailey, S.D., and Lancaster, N., 2000a. The sedimentary structure of linear sand dunes. Nature 406, 56-59.

Bristow, C.S., Chroston, P.N., and Bailey, S.D., 2000b. The structure and development of foredunes on a locally prograding coast: insights from ground-penetrating radar surveys, Norfolk, UK. Sedimentology 47, 923-944.

Bristow, C.S., Lancaster, N., and Duller, G.A.T., 2005. Combining ground penetrating radar surveys and optical dating to determine dune migration in Namibia. Journal of the Geological Society 162, 315-321.

Bruun, P., 1988. The Bruun Rule of Erosion by Sea-level Rise - A Discussion on Large-scale Two-Dimensional and 3-Dimensional Usages. Journal of Coastal Research 4, 627-648.

Buynevich, I.V., Bitinas, A., and Pupienis, D., 2007a. Lithological anomalies in a relict coastal dune: Geophysical and paleoenvironmental markers. Geophysical Research Letters 34.

Buynevich, I.V., FitzGerald, D.M., and Goble, R.J., 2007b. A 1500 yr record of North Atlantic storm activity based on optically dated relict beach scarps. Geology 35, 543-546.

Chauhan, O.S., 1992. Laminae and grain-size measures in beach sediments, East-coast beaches, India. Journal of Coastal Research 8, 172-182.

Cooper, J.A.G., Pilkey, O.H., 2004. Sea-level rise and shoreline retreat: time to abandon the Bruun Rule. Global and Planetary Change 43, 157-171.

Davidson-Arnott, R.G.D., 2005. Conceptual model of the effects of sea level rise on sandy coasts. Journal of Coastal Research 21, 1166-1172.

Davis, J.L., Annan, A.P., 1989. Ground penetrating radar for high resolution mapping of soil and rock stratigraphy. Geophysical Prospecting 37, 531-551.

Dickinson, K.A., 1971. Grain-size distribution and the deposition of northern Padre Island, Texas. U.S. Geological Survey Professional Paper. p. 750-C: C1-C6.

Fisk, H.N., 1959. Padre Island and the Laguna Madre flats, coastal South Texas. 2nd Coastal Geography Conference, Louisiana State University, p. 103-151.

Folk, R.L., 1966. A Review of Grain-Size Parameters. Sedimentology 6, 73-93.

Folk, R.L., Ward, W.C., 1957. Brazos River Bar: A Study in the Significance of Grain Size Parameters. Journal of Sedimentary Petrology 27, 3-26.

Garrison, J.R., Williams, J., Miller, S.P., Weber, E.T., McMechan, G., and Zeng, X.X., 2010. Ground-penetrating radar study of north Padre Island: Implications for barrier island internal architecture, model for growth of progradational microtidal barrier islands, and Gulf of Mexico sea-level cyclicity. Journal of Sedimentary Research 80, 303-319.

Hayes, M.O., 1964. Grain size modes in Padre Island sands. In: Depositional Environments-South-Central Texas coast. Gulf Coast Assoc. Geol. Soc., Annu. Mtg., Austin, Texas, Field Trip Guidebook, pp. 121-126.

Hesp, P., 1988. Morphology, dynamics and internal stratification of some established foredunes in southeast Australia. Sedimentary Geology 55, 17-41.

Houser, C., 2009. Synchronization of transport and supply in beach-dune interaction. Progress in Physical Geography 33, 733-746.

Houser, C., Hapke, C., and Hamilton, S., 2008. Controls on coastal dune morphology, shoreline erosion and barrier island response to extreme storms. Geomorphology 100, 223-240.

Houser, C., Mathew, S., 2011. Alongshore variation in foredune height in response to transport potential and sediment supply: South Padre Island, Texas. Geomorphology 125, 62-72.

Hughes, G.M.a.M.G., 2003. Introduction to Coastal Processes & Geomorphology. Hodder Education, London.

Inman, D., L., 1949. Sorting of sediments in the light of fluid mechanics. Journal of Sedimentary Petrology 19, 51-70.

Inman, D., L., 1952. Measures for describing the size distribution of sediments. Journal of Sedimentary Petrology 22, 125-145.

Jol, H., Bristow, C., 2003. GPR in sediments: advice on data collection, basic processing and interpretation, a good practice guide. Geological Society 211, 9-27.

Jorgensen, W.R., 2007. A Validation of ground penetrating radar for reconstructing the internal structure of a rock glacier: Mount Mestas, Colorado, USA. Master's Thesis, Texas A&M University, College Station, Texas.

Knight, R., 2001. Ground penetrating radar for environmental applications. Annual Review of Earth and Planetary Sciences 29, 229-255.

Krumbein, W., C., 1938. Size frequency distribution of sediments and the normal phi curve. Journal of Sedimentary Petrology 8, 84-90.

Leoni, L., Sartori, F., Saitta, M., Damiani, V., Ferretti, O., and Viel, M., 1991. Mineralogy, chemistry, and grain-size composition of recent sediments in the Northern Tyrrhenian Sea - Contribution to the study of sediment transport and distribution. Environmental Geology and Water Sciences 17, 23-46.

Mason, C.C., Folk, R. L., 1958. Differentiation of beach, dune and aeolian flat environments by size analysis, Mustang Island, Texas. Journal of Sedimentary Petrology 28, No. 2, 211-226.

McBride, E.F., Abel-Wahab, A., and McGilvery, T.A., 1996. Loss of sand-size feldspar and rock fragments along the South Texas Barrier Island, USA. Sedimentary Geology 107, 37-44.

McCammon, R., B., 1962. Efficiencies of percentile measures for describing the mean size and sorting of sedimentary particles. Journal of Geology 70, 453-465.

McGourty, J., Wilson, P., 2000. Investigating the internal structure of Holocene coastal sand dunes using ground-penetrating radar: Example from the north coast of Northern Ireland. Proceedings of the Eighth International Conference on Ground Penetrating Radar 2000, University of Queensland, Australia, pp. 14-19.

Morton, R.A., Sallenger, A.H., 2003. Morphological impacts of extreme storms on sandy beaches and barriers. Journal of Coastal Research 19, 560-573.

Neal, A., 2004, Ground-penetrating radar and its use in sedimentology: principles, problems and progress. Earth-Science Reviews 66, 261.

Neal, A., Roberts, C.L., 2000. Applications of ground-penetrating radar (GPR) to sedimentological, geomorphological and geoarchaeological studies in coastal environments, In Pye, K., Allen, J.R.L., (Eds.), Coastal and estuarine

environments. Sedimentology, geomorphology and geoarchaeology. Volume 175: Geological Society Special Publication, p. 139-171.

Otto, G., H., 1939. A modified logarithmic probability graph for the interpretation of mechanical analyses of sediments. Journal of Sedimentary Petrology 9, 62-75.

Psuty, N.P., 1988. Sediment budget and dune/beach interaction. Journal of Coastal Research 1-4.

Richter, T.O., van der Gaast, S., and Koster, B., 2006. The Avaatech XRF Core Scanner: technical description and applications to NE Atlantic sediments: New Techniques in Sediment Core Analysis. Geological Society, London, v. Special Publications, 267, p. 39-50.

Sallenger, A.H., 2000. Storm impact scale for barrier islands. Journal of Coastal Research 16, 890-895.

Sassen, D.S., Everett, M.E., 2009. 3D polarimetric GPR coherency attributes and full-waveform inversion of transmission data for characterizing fractured rock. Geophysics 74, J23-J34.

Sassen, D.S., Everett, M.E., and Munster, C.L., 2009. Ecohydrogeophysics at the Edwards Aquifer: insights from polarimetric ground-penetrating radar. Near Surface Geophysics 7, 427-438.

Schwartz, M.L., 2005, Encyclopedia of Coastal Science. Springer, Netherlands.

Schwartz, R.K., Birkemeier, W.A., 2004. Sedimentology and morphodynamics of a barrier island shoreface related to engineering concerns, Outer Banks, NC, USA. Marine Geology 211, 215-255.

Sensors & Software, 2001. Win_EKKO User's Guide Version 1.0. Sensors and Software. Mississauga, Canada.

Sharma, P.V., 1997. Environmental and Engineering Geophysics. Cambridge University Press, Cambridge, U.K. p 475.

Sherman, D.J., 1995. Problems of scale in the modeling and interpretation of coastal dunes. Marine Geology 124, 339-349.

Sherman, D.J., Bauer, B.O., 1993. Dynamics of beach-dune systems. Progress in Physical Geography 17, 413-447.

Sherman, D.J., Lyons, W., 1994. Beach-state controls on aeolian sand delivery to coastal dunes: Physical Geography 15, 381-395.

Short, A.D., 1984. Beach and nearshore facies - Southeast Australia. Marine Geology 60, 261-282.

Short, A.D., Hesp, P.A., 1982. Wave, beach and dune intearactions in Southeastern Australia. Marine Geology 48, 259-284.

Trask, P., D., 1932. Origin and Environment of Source Sediments of Petroleum. Gulf Publishing Company, Houston, Texas. 323 pp.

Von Eynatten, H., Tolosana-Delgado, R., 2011. Geochemistry versus grain-size relations of sediments in the light of comminution, chemical alteration, and contrasting source rocks. Proceedings of the 4th International Workshop on Compositional Data Analysis 2011, Girona, Spain, pp. 1-12.

Weise, B.R., White, W. A., 1980. Padre Island National Seashore: guide to the geology, natural environments, and history of a Texas barrier island. Bureau of Economic Geology, Austin, TX.

Wright, L.D., Chappell, J., Thom, B.G., Bradshaw, M.P., Cowell, P., 1979. Morphodynamics of reflective and dissipative beach and inshore systems: Southeastern Australia. Marine Geology 32, 105-140.

Wright, L.D., Short, A.D., 1984. Morphodynamic variability of surf zones and beaches: a synthesis. Marine Geology 56, 93-118.

Yang, S.Y., Lim, D.I., Jung, H.S., and Oh, B.C., 2004. Geochemical composition and provenance discrimination of coastal sediments around Cheju Island in the southeastern Yellow Sea. Marine Geology 206, 41-53.

APPENDIX

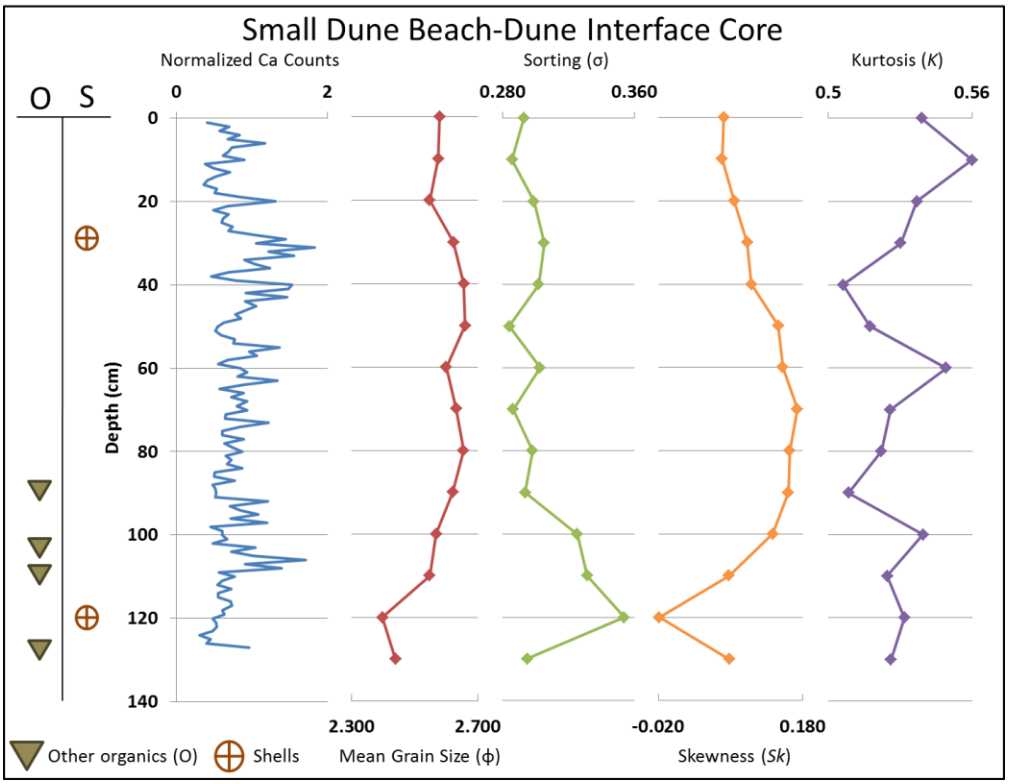

Figure 28. Small dune beach-dune interface core plot showing visible organic layers, normalized Ca counts and grain size parameters.

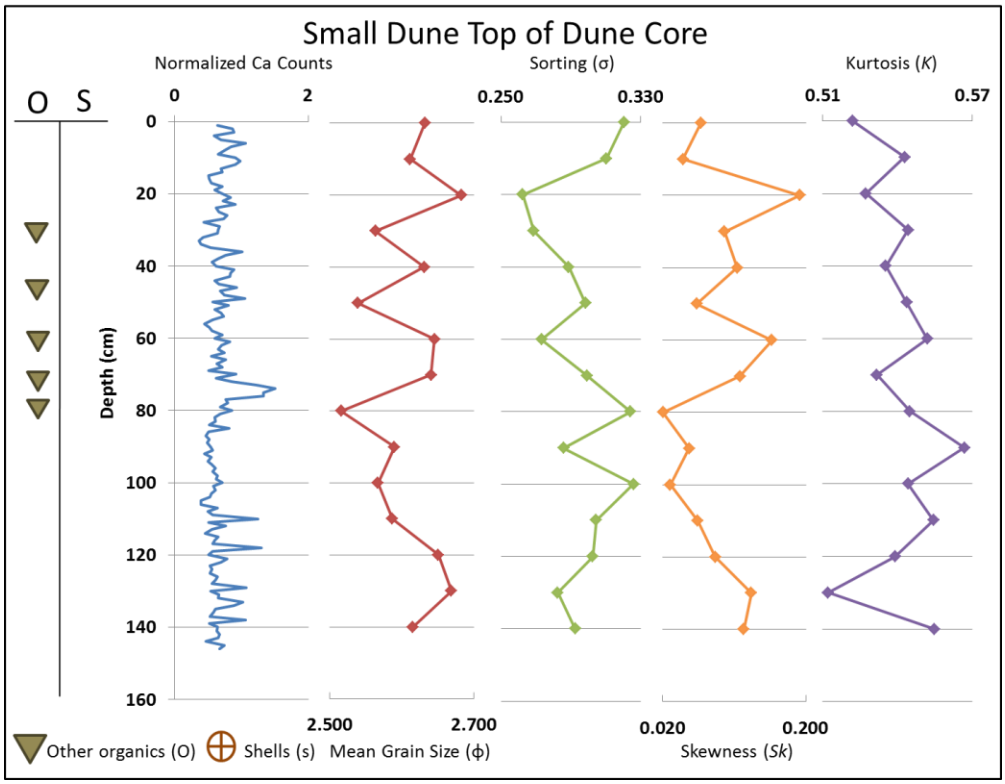

Figure 29. Small dune top of dune core plot showing visible organic layers, normalized Ca counts and grain size parameters.

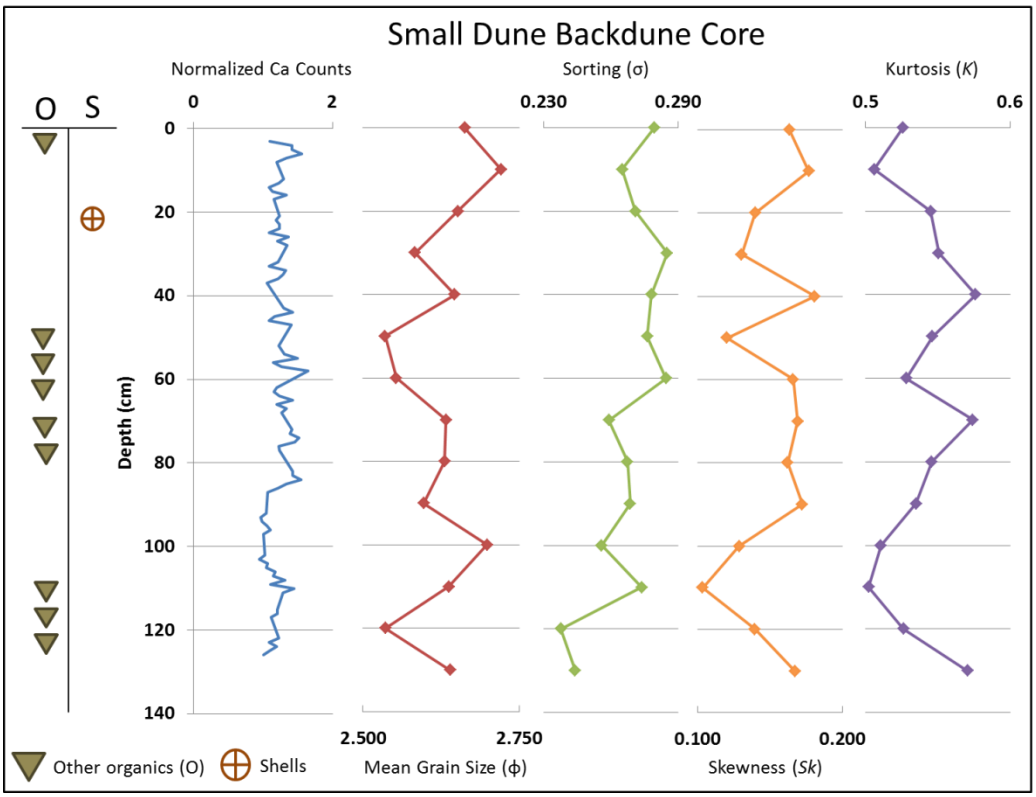

Figure 30. Small dune backdune core plot showing visible organic layers, normalized Ca counts and grain size parameters.

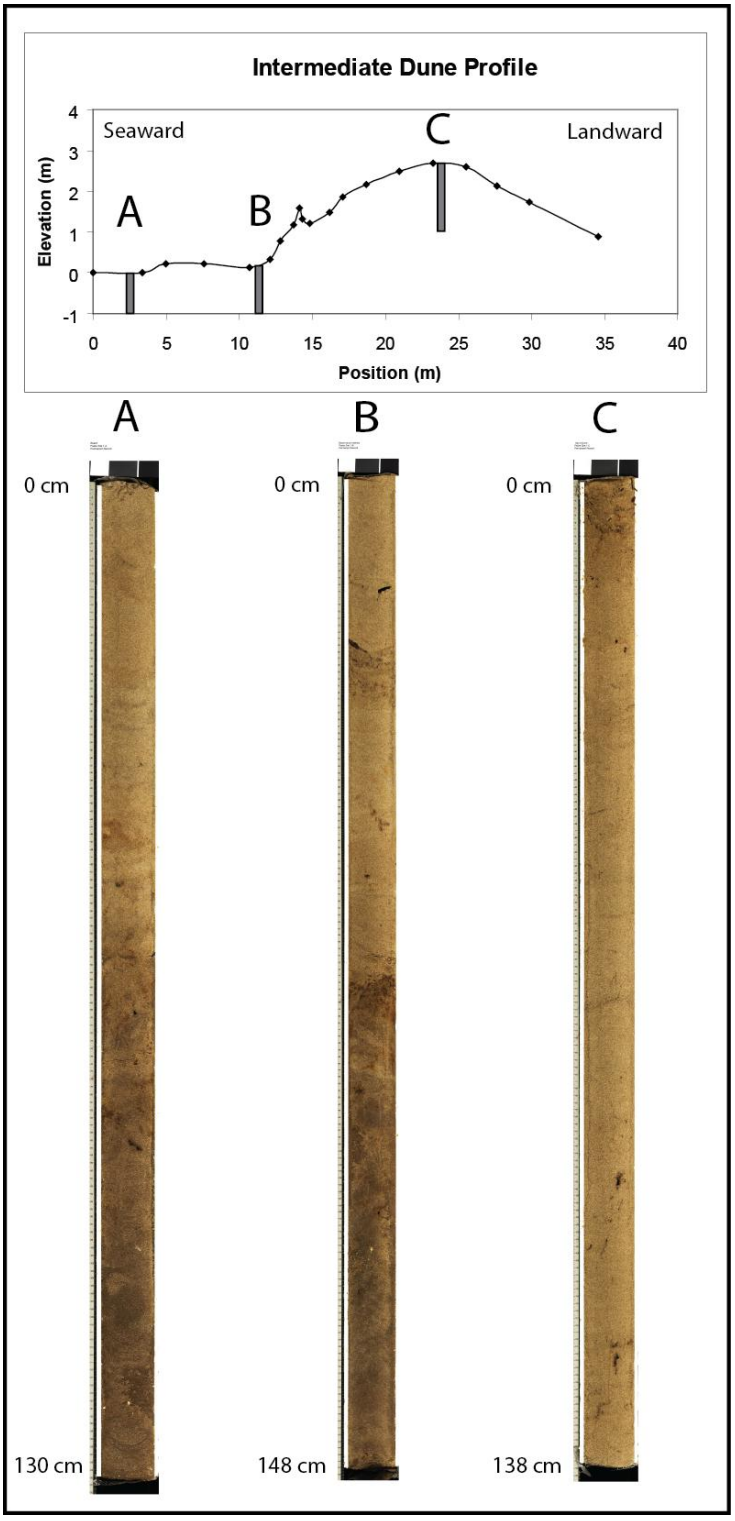

Figure 31.Intermediate dune site vibra-cores and beach profile, showing relative locations. A) Beach, B) Beach-dune interface and C) Top of Dune.

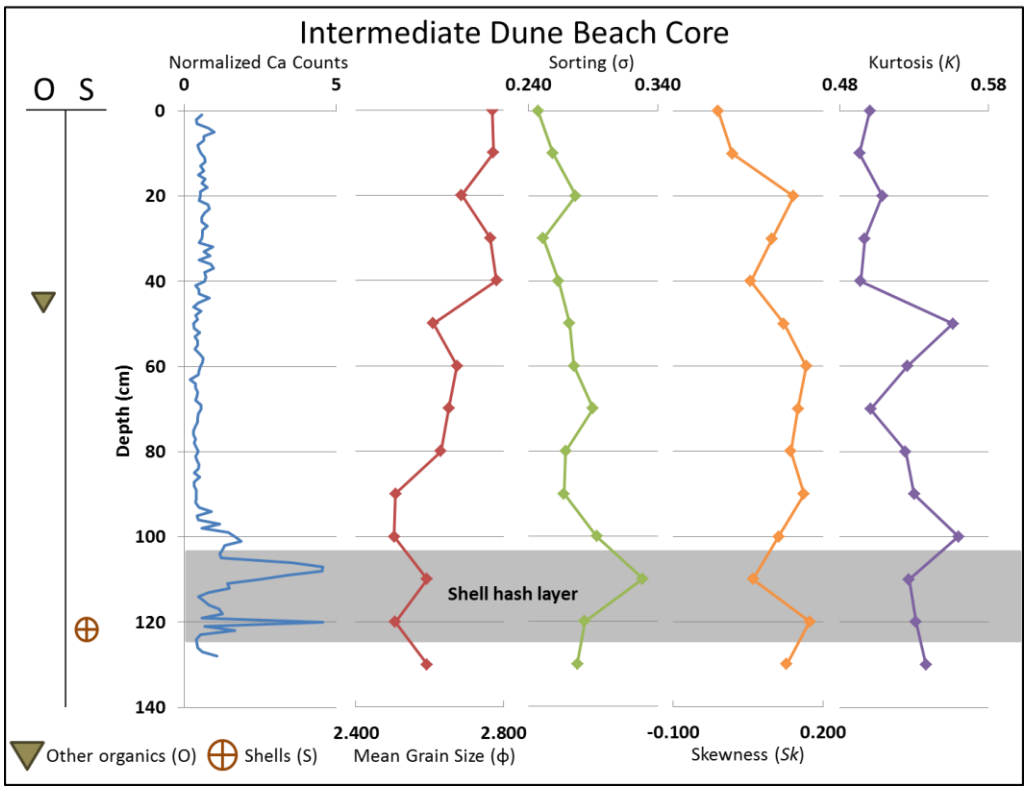

Figure 32. Intermediate dune beach core plot showing visible organic layers, normalized Ca counts and grain size parameters.

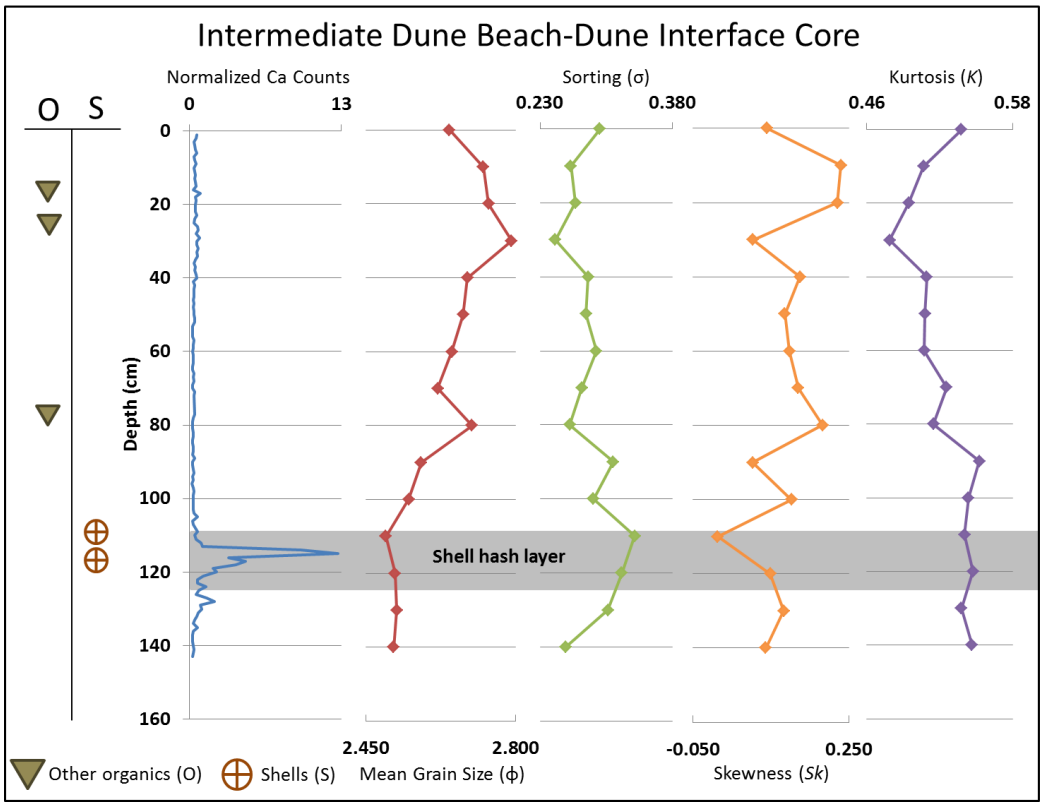

Figure 33. Intermediate dune beach-dune interface core plot showing visible organic layers, normalized Ca counts and grain size parameters.

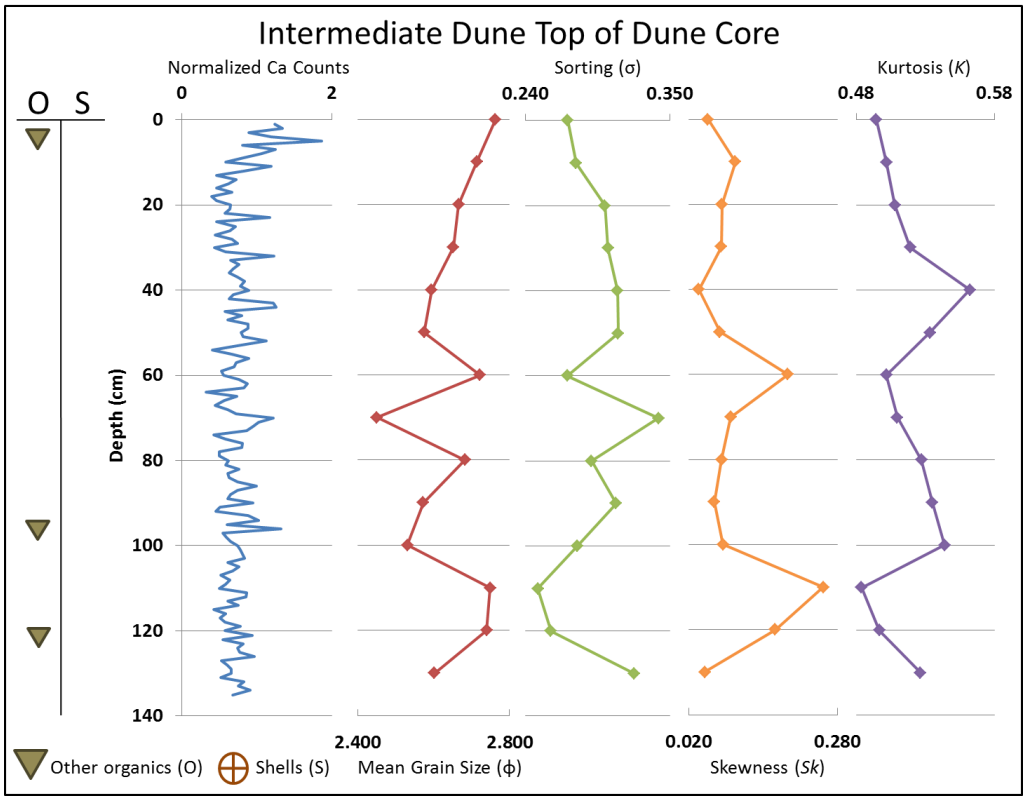

Figure 34. Intermediate dune top of dune core plot showing visible organic layers, normalized Ca counts and grain size parameters.

Figure 35. Large dune site vibra-cores and beach profile, showing relative locations. A) Beach, B) Beach-duplicate, C) Beach-dune interface and D) Backdune.

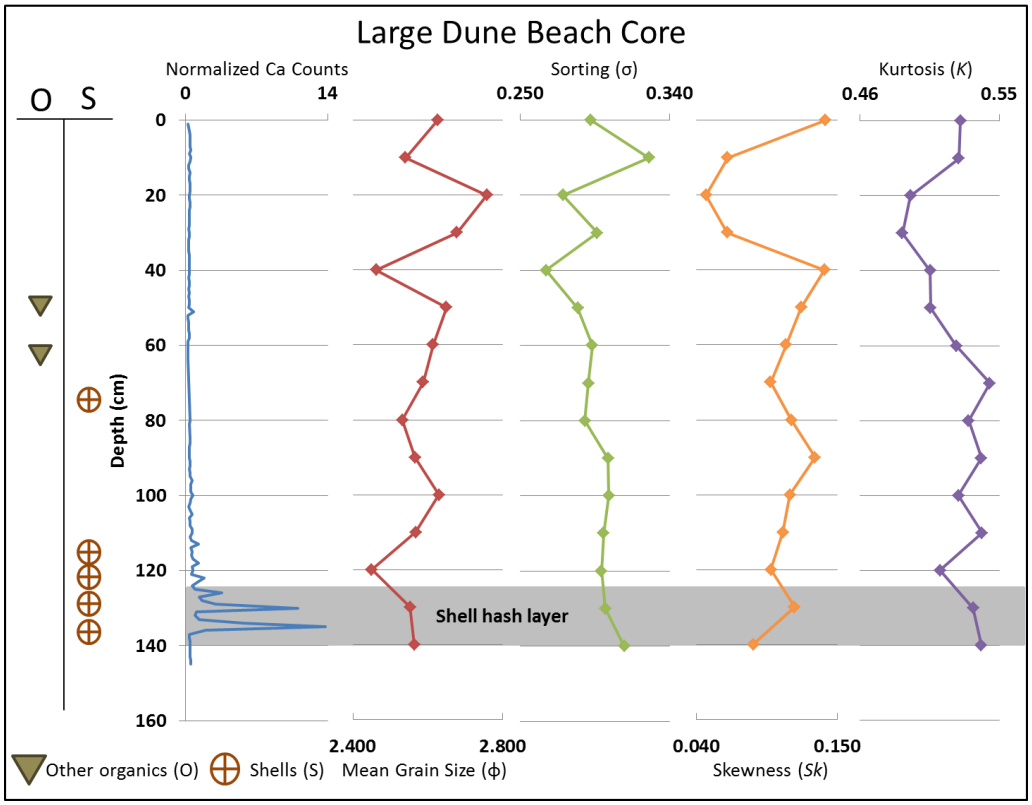

Figure 36. Large dune beach core plot showing visible organic layers, normalized Ca counts and grain size parameters.

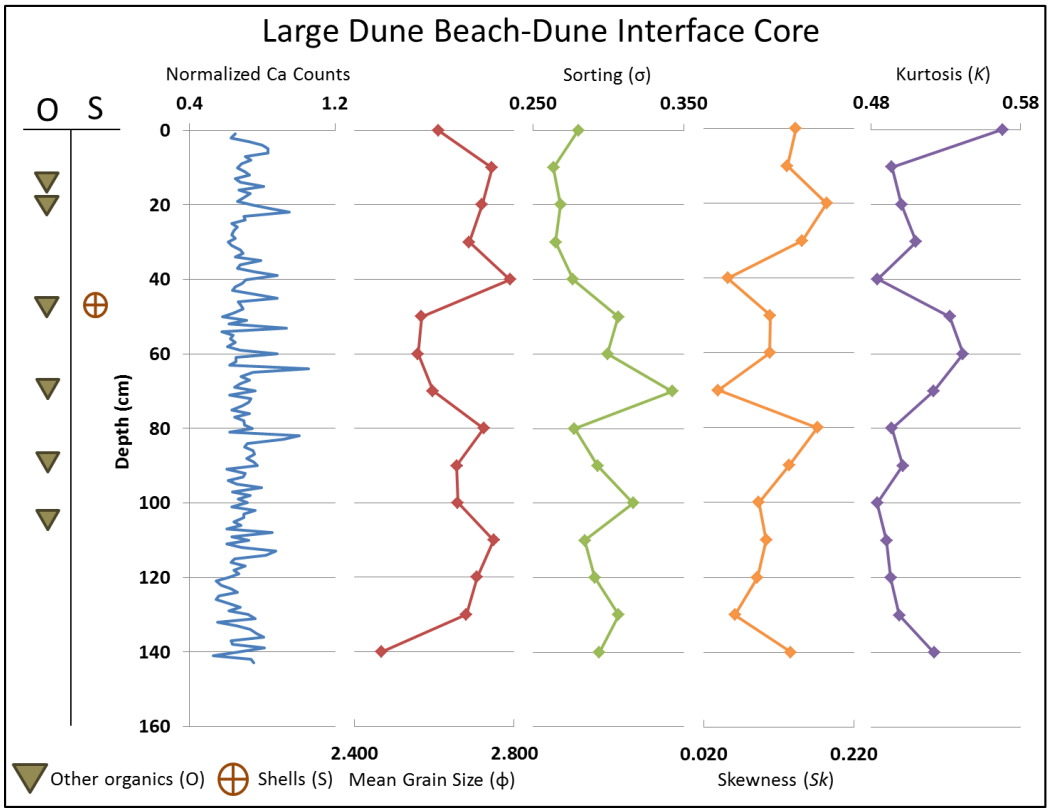

Figure 37. Large dune beach-dune interface core plot showing visible organic layers, normalized Ca counts and grain size parameters.

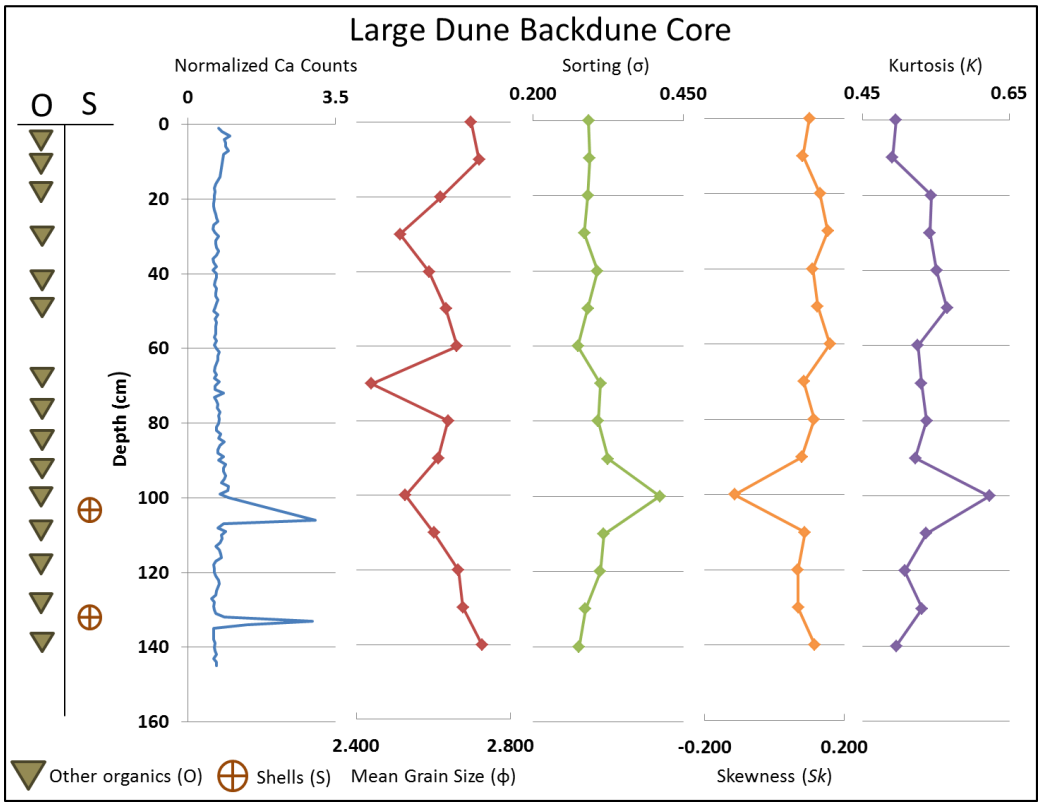

Figure 38. Large dune backdune core plot showing visible organic layers, normalized Ca counts and grain size parameters.

VITA

Bradley Allen Weymer
The Department of Geology and Geophysics
Texas A&M University
College Station, TX 77843-3115
brad.weymer@gmail.com

EDUCATION

Texas A&M University, College Station, Texas — May 2012
M.S. Geology

Millersville University, Millersville, Pennsylvania — December 2004
B.S. Oceanography

EMPLOYMENT

- Graduate Assistant Researcher: San Andreas Fault Observatory at Depth (SAFOD) curator. College Station, Texas. (June 5, 2008 – May, 2012).
- Laboratory Technician: TDI Brooks International, College Station, Texas. PMEX Expedition. Tampico, Mexico (April 27- May 8, 2008).
- Research Assistant: Integrated Ocean Drilling Program (IODP). Scientific Ocean Drilling Vessel (SODV) project. College Station, Texas (January 29, 2007 – April 7, 2008), (March 10 – May 19, 2006).
- Independent Contractor: National Gas Hydrate Program of India (NGHP) Expedition 1 Legs 3a, 3b, and 4. Chennai, India. (June 8 – August 17, 2006).
- Marine Laboratory Specialist: IODP Expeditions 307, 309,312 (April 25 – May 30, 2005), (July 8 – August 28, 2005), (October 28, 2005 – January 10, 2006).
- Natural Resource Technician III: Maryland Department of Natural Resources (MDNR). Annapolis, Maryland (March – July 2005).

SELECTED PUBLICATIONS/PRESENTATIONS

- Weymer, B., Firth, J., Rumford, P., Chester, F., Chester, J., Lockner, D., 2011. SAFOD Phase III Core Sampling and Data Management at the Gulf Coast Repository. *Sci.Drill*. 11:48-50, doi:10.2204/iodp.sd.11.06.2011.
- American Geophysical Union Annual Meeting, San Francisco, CA December 2010. Poster: "Using Ground-Penetrating Radar (GPR) to Investigate Beach-Dune Interaction at North Padre Island, Texas."
- American Association of Petroleum Geologist Annual Meeting, New Orleans, LA. April 2010. Poster: "The Unconfined Compressive Strength of SAFOD Core from Point-Load Penetrometer Tests."
- Weymer, B., "Drill Ship Glomar Challenger", "Drill Ship JOIDES Resolution", and "The Deep-Sea Drilling Project." In: Nichols, Charles R., and Robert G. Williams, *Encyclopedia of Marine Science, New York: Facts on File*. 2009.